Published in final edited form as:
J Comp Neurol. 2014 June 15; 522(9): 2053–2074. doi:10.1002/cne.23517.

PROJECTION NEURONS OF THE VESTIBULO-SYMPATHETIC REFLEX PATHWAY

Gay R. Holstein[1,2], **Victor L. Friedrich Jr**[2], and **Giorgio P. Martinelli**[1]

[1]Department of Neurology, Icahn School of Medicine at Mount Sinai; New York, NY 10029

[2]Department of Neuroscience, Icahn School of Medicine at Mount Sinai; New York, NY 10029

Abstract

Changes in head position and posture are detected by the vestibular system and are normally followed by rapid modifications in blood pressure. These compensatory adjustments, which allow humans to stand up without fainting, are mediated by integration of vestibular system pathways with blood pressure control centers in the ventrolateral medulla. Orthostatic hypotension can reflect altered activity of this neural circuitry. Vestibular sensory input to the vestibulo-sympathetic pathway terminates on cells in the vestibular nuclear complex, which in turn project to brainstem sites involved in the regulation of cardiovascular activity, including the rostral and caudal ventrolateral medullary regions (RVLM and CVLM, respectively). In the present study, sinusoidal galvanic vestibular stimulation was used to activate this pathway, and activated neurons were identified through detection of c-Fos protein. The retrograde tracer FluoroGold was injected into the RVLM or CVLM of these animals, and immunofluorescence studies of vestibular neurons were conducted to visualize c-Fos protein and FluoroGold concomitantly. We observed activated projection neurons of the vestibulo-sympathetic reflex pathway in the caudal half of the spinal, medial and parvocellular medial vestibular nuclei. Approximately two-thirds of the cells were ipsilateral to FluoroGold injection sites in both RVLM and CVLM and the remainders were contralateral. As a group, cells projecting to RVLM were located slightly rostral to those with terminals in CVLM. Individual activated projection neurons were multipolar, globular or fusiform in shape. This study provides the first direct demonstration of the central vestibular neurons that mediate the vestibulo-sympathetic reflex.

Keywords

vestibular; orthostatic hypotension; RVLM; blood pressure

Corresponding author: Dr. Gay R. Holstein, Box 1140; Dept. Neurology, Annenberg 20-06e, Icahn School of Medicine at Mount Sinai, One Gustave Levy Place, New York, NY 10029, (T): 212-241-7072, (F): 212-987-3937, gay.holstein@mssm.edu.

CONFLICTS OF INTEREST

The authors have no conflicts of interest.

ROLES OF AUTHORS

All authors had full access to all the data in the study and take responsibility for the integrity of the data and the accuracy of the data analysis. Study concept and design: GRH, VLF, GPM. Acquisition of data: GRH, GPM. Analysis and interpretation of data: GRH, VLF. Drafting of the manuscript: GRH. Critical revision of the manuscript for important intellectual content: GRH, VLF, GPM. Statistical analysis: VLF. Obtained funding: GRH, VLF, GPM. Administrative, technical, and material support: GRH, VLF, GPM. Study supervision: GRH, VLF, GPM.

INTRODUCTION

The vestibular system is a multifaceted sensorimotor integrative complex that is critical for normal balance, equilibrium, spatial orientation, gaze stability, postural control and compensatory autonomic adjustments in response to changes in posture and movement (for reviews, see (Angelaki and Cullen, 2008; Holstein, 2012)). The peripheral receptors sense head motion or head position in three-dimensional space, and convey this information to one or more of the four main cell groups comprising the vestibular nuclear complex (VNC), as well as to accessory vestibular nuclear groups and the cerebellum. Functionally, there are five main vestibular effector pathways supporting the critical functions of the system: vestibulo-ocular, vestibulo-spinal, vestibulo-colic, vestibulo-thalamo-cortical and vestibulo-sympathetic “reflexes”. In the present study, we investigated VNC neurons that participate in vestibulo-sympathetic pathways involved in the control of blood pressure.

Homeostatic control of blood pressure is mediated through the baroreflex, which transmits baroreceptor signals to the solitary nucleus (Spyer, 1981), and from there to the caudal ventrolateral medullary region (CVLM) and nucleus ambiguus. The CVLM gives rise to both excitatory and GABAergic inhibitory projections to the rostral ventrolateral medulla (RVLM) (Blessing, 1988; Jeske et al., 1995; Natarajan and Morrison, 2000), an area containing presympathetic neurons that innervate the intermediolateral cell column in the spinal cord (for reviews, see (Blessing, 2004; Guyenet, 2006; Pilowsky and Goodchild, 2002; Sved et al., 2003)). This pathway maintains homeostasis through constant negative feedback activity. In contrast, the vestibular system appears to influence blood pressure through a more direct and feed-forward mechanism that modulates blood pressure during changes in posture with respect to gravity (e.g. when rising from a seated or lying position) in order to maintain adequate blood flow to the brain (Dieterich and Brandt, 2010; Serrador et al., 2009). The existence of a functional connection between the vestibular system and blood pressure control mechanisms was hypothesized almost a century ago (Bradbury and Eggleston, 1925) and is now supported by a body of basic and clinical research (see Figure 1).

It has been proposed that two general regions of the VNC give rise to vestibulo-sympathetic pathways (Balaban and Yates, 2004). Connections with limbic and hypothalamic areas may be derived from neurons located rostrally in the superior vestibular nucleus and medial vestibular nucleus (MVN) (Balaban, 1996; Kerman et al., 2006). In contrast, vestibular influences on blood pressure, heart rate, respiration and digestion reportedly originate from cells in the caudal portion of MVN and in the spinal vestibular nucleus (SpVN). Early studies found that the primary medullary targets of this latter pathway include subregions of the solitary nucleus and the dorsal motor vagal nucleus, with only minor vestibular projections noted in nucleus ambiguus, raphé magnus, RVLM and CVLM (Balaban and Beryozkin, 1994; Porter and Balaban, 1997; Ruggiero et al., 1996; Yates et al., 1994). However, the behavioral and cellular physiological studies suggest that vestibular and baroreflex signals are integrated at the level of the RVLM (Yates and Bronstein, 2005; Yates et al., 1994). Concordantly, our laboratory demonstrated a substantial direct projection from the caudal VNC to the ventrolateral medulla (Holstein et al., 2011). Since these projections could provide a scaffold for more direct modifications of sympathetic nerve activity as are

required to compensate for rapid changes in posture and locomotion (for example, see (Voustianiouk et al., 2006)), the present study was conducted to investigate the functional activity of this caudal vestibulo-sympathetic pathway.

The VNC is comprised of a multiplicity of cell types. Subpopulations of this neuronal pool have been parsed on the basis of location, cytoarchitecture, functional connectivity, physiological signatures, chemoanatomy, and marker genes (Bagnall et al., 2007; Kodama et al., 2012) (for review, see (Highstein and Holstein, 2006)). One approach that has been used successfully to identify some types of stimulated vestibular neurons involves the visualization of c-Fos, the protein product resulting from activation of the immediate early gene *c-fos*. Using this approach, activated VNC neurons have been identified following horizontal and vertical linear acceleration, Ferris wheel rotation, off-vertical-axis rotation, centrifugation, spaceflight, and steps of galvanic vestibular stimulation (GVS) (Abe et al., 2009; Baizer et al., 2010; Cai et al., 2007; Cai et al., 2010; Chen et al., 2003; Fuller et al., 2004; Gustave Dit Duflo et al., 2000; Kaufman, 2005; Kaufman et al., 1992; 1993; Kaufman and Perachio, 1994; Lai et al., 2004; Lai et al., 2008; Lai et al., 2006; Marshburn et al., 1997; Pompeiano et al., 2002; Saxon et al., 2001; Tse et al., 2008; Zhang et al., 2005). We previously examined c-Fos protein accumulation in neurons activated by low-frequency binaural sinusoidal GVS (sGVS), an effective stimulus for the vestibulo-sympathetic reflex (Cohen et al., 2011a; Cohen et al., 2013; Cohen et al., 2011b; 2012; Holstein et al., 2012), and found activated vestibular neurons in SpVN, MVN, and a small medial area of the superior vestibular nucleus. The highest density of sGVS-activated c-Fos-positive vestibular neurons was observed in MVN; immunolabeled cells were distributed throughout the entire rostro-caudal extent of this nucleus, although they were predominantly located in the caudal and parvocellular regions (Holstein et al., 2012). The present study was conducted to determine whether sGVS-activated VNC neurons have direct projections to RVLM and/or CVLM. By combining functional mapping and classical tract tracing, we sought to identify the VNC neurons of the vestibulo-sympathetic pathway involved in blood pressure control.

MATERIALS AND METHODS

All experiments were approved by the Institutional Care and Use Committee at Mount Sinai and were conducted in accordance with the National Institutes of Health Guide for the Care and Use of Laboratory Animals (Eighth Edition, 2011). Twenty adult male Long-Evans rats (Harlan Laboratories, MA) weighing 300–400g were used for these studies. Ten of these animals received tracer injections and sGVS stimulation, and were used for double-label immunofluorescence studies of activated vestibular projection neurons. An additional eight rats were used for sGVS/c-Fos control studies: four of these rats received sGVS stimulation and the other four did not. The remaining two rats were used for technical purposes such as screening primary antibodies, determining optimal antibody dilutions and assessing secondary antibody sensitivities.

sGVS—Ag/AgCl needle electrodes (BAK) connected to a computer-controlled current stimulator (Cohen et al., 2011a) were inserted under the skin over the mastoids, behind the external auditory meati of isoflurane-anesthetized (4% induction; 2% maintenance) animals.

An individual sGVS stimulus consisted of a set of five cycles of binaural current given at 2 mA and a frequency of 0.025 Hz. This stimulus was repeated 5 times with three min rest periods between repetitions. Rats were then allowed to recover from anesthesia and were euthanized by perfusion with mixed buffered aldehydes under isoflurane anesthesia 90 min after the cessation of the last stimulus.

sGVS controls—Control rats for the sGVS stimulation did not receive FluoroGold injections. These subjects were anesthetized and positioned in the cylindrical holder for sGVS testing. Ag/AgCl needle electrodes were placed and connected to the current stimulator as described above, but no current was applied. All subsequent animal and immunoperoxidase tissue treatments were identical for the sGVS-stimulated and non-stimulated subjects. Immunoperoxidase-diaminobenzidine was used for detection of c-Fos in these sections because it is generally a more sensitive detection system than routine immunofluorescence. The number of c-Fos-positive cells in MVN and in SpVN were counted using 50 μm thick Vibratome sections between Bregma −12.6 and −11.4 from four sGVS-stimulated and three non-stimulated control rats. Sections from each animal were at least 250 μm apart, and counts from the two sides of the brainstem were combined. The mean number of cells/section/VNC region for each animal was used for statistical analysis. Since inspection revealed an obvious dependence of group standard deviation on the group mean, data were log-transformed for the t-test comparisons.

Blood pressure and heart rate measurements—Peripheral blood pressure was measured by photoplethysmography (PPG), a non-invasive optical technique used to detect blood volume changes at the surface of the skin using a small sensor clamped on a paw (Holstein et al., 2012). The PPG signal is composed of two major factors: peripheral blood pressure and vasoconstriction (Imholtz et al., 1991). This signal was passed through a bandpass filter that augmented the heart beat component, and then the high frequency noise was removed offline. Previous studies (Cohen et al., 2011a) have demonstrated that changes in blood pressure and heart rate can be detected using PPG data.

In the present study, PPG was used to verify that the sGVS stimulus exerted an impact on sympathetic activity. Previous studies have shown that GVS activates the vestibular nerve (for review, see (Curthoys, 2010)), and have documented the effects of parametric variation of sGVS on heart rate and blood pressure, the range and magnitude of responses elicited by these stimuli, and the influence of anesthesia on these autonomic responses (Cohen et al., 2011a; Cohen et al., 2013). The degree of specificity of low frequency 2 mA sGVS for activating vestibulo-sympathetic pathways has also been addressed previously (Cohen et al., 2011b; 2012; Curthoys and MacDougall, 2012), and the ability to visualize sGVS-activated neurons using c-Fos localization has been demonstrated (Holstein et al., 2012). All 10 experimental animals used for the double label immunofluorescence study showed modulations in heart rate and blood pressure associated with the sGVS stimulation, reflecting stimulus-specific activation of the vestibulo-sympathetic pathway.

Tracer injections—Each animal was anesthetized with isoflurane (4% induction, 2% maintenance), shaved and secured in a computer-assisted stereotaxic frame (Leica *Angle Two*™, Leica Microsystems, St Louis, MO). The animal was kept normothermic by resting it

on a heating pad regulated by feedback from a rectal thermometer. The eyes were kept moist with an ophthalmic ointment, and an analgesic was administered preemptively (Buprenex 0.05mg/kg, SQ; Reckitt Benckiser Pharmaceuticals; Richmond VA). The animal was then prepared for aseptic surgery by draping it and disinfecting the head and neck with Povidone. A midline incision was placed from the top on the skull to the atlas region. The periosteum was removed and the occipital bone and the atlanto-occipital membrane were exposed by blunt dissection and retraction of the neck muscles. A glass pipette (tip OD: ~20–25 μm) filled with 2% FluoroGold diluted in saline (Fluorochrome, LLC, Denver, CO) was mounted on the *Angle Two* dorsoventral drive (DV) tilted 45° over the horizontal plane. After entering the target coordinates for RVLM (ML: ±2.34; AP: −12.24; DV: −10.21) or CVLM (ML: ±22; AP: −12.80; DV: −10.0) (Paxinos and Watson, 2009) in the computer, the pipette tip was positioned at Bregma. Using computer assistance, the *Angle Two* AP and ML drives were then adjusted and the pipette was advanced toward the target area in the brainstem via a small burr hole (~2 mm in diameter) drilled at ML ± 2.3 mm and slightly above the atlanto-occipital membrane. The tracer was iontophoresed for 10 min at +5 μA (7 sec on, 7 sec off). At the end of the iontophoresis, the pipette was left *in situ* for 2 min and then slowly withdrawn. After the injection, the neck muscles were approximated with interrupted stitches (4.0 silk) and the skin was closed with surgical clips. The rat received 3 ml of sterile saline SQ at the end of the procedure. The analgesic Buprenex was administered (SQ, 0.05 mg/kg) twice a day for three days. Animals were allowed to recover for 10 days before the terminal experiment was conducted.

Tissue harvesting and processing

Perfusion, fixation and tissue sectioning—While peak c-Fos protein accumulation has been demonstrated 90 – 240 min after stimulation, most studies report maximal expression at 90–120 min and decreased expression at shorter and longer times (for reviews, see (Durchdewald et al., 2009; Kovács, 2008)). For this reason, rats were anesthetized with isoflurane and perfused transcardially 90 min after the completion of the sGVS stimulation with 100 ml of 37°C 10 mM phosphate buffered saline (PBS) followed by 500 ml of 4% paraformaldehyde/0.2% glutaraldehyde fixative in 0.1M phosphate buffer (pH 7.4) at room temperature. Brains were harvested immediately after perfusion, cut into blocks using an adult rat brain coronal matrix (Ted Pella, Inc.; Redding, CA), and stored at 4°C in PBS with 0.02% NaN_3. A vibrating microtome was then used to cut the blocks into 50 μm thick serial sections that extended through the entire VNC and ventrolateral medullary region. These sections (usually about 120 per animal) were stored in PBS with 0.02% NaN_3 at 4°C.

Anatomical boundaries—The presence and location of the four main vestibular nuclei (spinal, medial, lateral and superior) were determined for each tissue section by comparison of the anatomical landmarks present on the dorsal aspect of the section with standard atlas sections (Paxinos and Watson, 2005). The boundaries of the RVLM and CVLM were determined in each tissue section by comparison of the structures present ventrally in the section with published maps and atlases of those regions (Bourassa et al., 2009; Card et al., 2006; Goodchild and Moon, 2009; Paxinos and Watson, 2005; 2009). Utilizing the most conservative estimates based on these published maps, we identified the RVLM as the 1 mm rostrocaudal region extending from approximately 11.8 mm to 12.8 mm caudal to Bregma.

The other dimensions of the region were defined by a triangle with pars compacta of nucleus ambiguus at the apex, and the ventral surface of the medulla 1.4 and 2.2 mm lateral to the midline as the two other geometric points. The CVLM region was also defined by anatomical coordinates, and extended from 12.8 mm to 13.6 mm caudal to Bregma. As previously noted (Goodchild and Moon, 2009), these regions correspond well with published functional and physiological maps of RVLM and CVLM.

Primary antibodies—Three commercial antibodies against c-Fos were evaluated for this study: two rabbit polyclonal antisera (Santa Cruz Biotechnology, Cat.# sc-253; Calbiochem, Cat.# PC38), and one rabbit polyclonal antiserum directly conjugated with AlexaFluor 488 (Santa Cruz Biotechnology, Cat.# sc-253 AF488) (Table 1). All three reagents stained the same VNC regions and cells. With our tissue fixation and processing conditions, however, the unlabeled polyclonal sera provided more robust labeling than the AlexaFluor 488-tagged polyclonal antiserum. Results using the two unlabeled polyclonal sera were indistinguishable. All data for this report were obtained using the rabbit anti-c-Fos polyclonal antiserum from Santa Cruz Biotechnology (Cat.# sc-253) diluted 1:500. In addition, some tissue sections were exposed to a mixture of this rabbit polyclonal antibody preabsorbed with blocking peptide Santa Cruz Biotechnology (Cat. sc-#253P) as a control for nonspecific staining. No label was present in these sections. FluoroGold was visualized using a commercial rabbit polyclonal antiserum (Millipore Cat. #AB153) to boost the fluorescence signal of this reagent. Both the c-Fos and FluoroGold primary antibodies provided staining of VNC regions and cells that conformed to previous publications (Holstein et al., 2011; Holstein et al., 2012).

Immunoperoxidase/diaminobenzidine staining—Vibratome sections were immersed in blocking buffer (BB: PBS containing 10% normal goat serum, 0.1% Triton X-100 and 0.02% NaN_3) for 4 – 6 h or overnight and then treated with anti-FluoroGold antibody (1:5000 in BB; 12 – 18 h) followed by PBS rinses (6 changes over 4 – 6 h) and peroxidase-conjugated goat anti-rabbit secondary antibody (Jackson ImmunoResearch Cat. #111-035-144; 1:2000 in BB without NaN_3). Sections were then rinsed in PBS (6 changes over 2 h) and incubated in 0.1M Tris buffer (pH 7.6) containing 0.5 mg/ml diaminobenzidine (DAB; Sigma D-5905; St. Louis, MO) with 0.01% H_2O_2 for 5–10 min at room temperature. The staining was stopped by multiple PBS rinses.

Immunofluorescence—Tissue sections were processed for immunofluorescence detection of c-Fos and FluoroGold, as well as DAPI staining to visualize the location and approximate size range of neuronal nuclei. Since both primary antibodies were raised in the same species - rabbit - we employed layered sequential applications of primary and secondary antibodies, using an Fab fragment secondary antibody to bind to the first primary in order to limit cross-reactive binding. Briefly, sections were exposed in the first layer to rabbit anti-c-Fos primary followed by labeled Fab fragment anti-rabbit IgG secondary. After blocking in high-concentration unlabeled Fab fragment anti-rabbit secondary, sections were exposed to rabbit anti-FluoroGold followed by anti-rabbit IgG secondary antibody labeled with a different fluorochrome.

Additional controls included tissue sections labeled with both secondaries but only one primary antibody, sections labeled with one or both secondaries but no primaries, and sections treated with the blocking and rinsing steps, but no antibody incubations. Each secondary antibody bound solely to its appropriate primary antibody; there was no binding to the inappropriate primary reagent. In addition, all of the immunofluorescence-stained sections contained profiles that were stained by only one of the colors in the specimen's secondaries mixture (see for example Figures 9 – 11). This provided further assurance within each individual section that only one secondary antibody bound to each primary antibody and therefore that secondary antibody cross-reactivity was insignificant.

All steps were performed at room temperature with agitation on an orbital shaker. Free-floating sections were pre-incubated for 3 – 6 h in BB; incubated for 12 – 18 h in rabbit anti-c-Fos primary antibody (1:500 in BB); washed for 4 – 8 h in multiple changes of PBS; incubated for 12 – 18 h in AlexaFluor®- or DyLite®-conjugated goat anti-rabbit IgG (H+L) secondary antibody Fab fragment (8 μg/ml in BB; JacksonImmunoResearch); washed for 4 – 8 h in multiple changes of PBS; fixed briefly with paraformaldehyde; washed again; exposed 12 – 18 h to unlabeled Fab fragment goat anti-rabbit IgG (20 μg/ml in BB; JacksonImmunoResearch); washed; treated 12 – 18 h with rabbit anti-FluoroGold primary antibody (1:400 in BB); washed; and treated with AlexaFluor-conjugated goat anti-rabbit IgG (H+L) (1:400 in BB; Invitrogen). Following this staining, sections were immersed in DAPI solution (300 nM in PBS) for 30 min. After the final washes, all sections were mounted on glass slides and coverslipped using Prolong (Invitrogen) mounting medium. Since we have experienced varying degrees of sensitivity among secondary antibodies, we used several different secondary antibodies and several alternative fluorochromes (in different sections) to detect each primary antibody.

Microscopy, stain analysis and image preparation—Sections were examined and images were acquired with a Zeiss Axioplan2 microscope equipped with structured illumination (ApoTome). The intensity of c-Fos staining in different subsets of labeled neurons was not compared or quantified in the sGVS stimulated animals because stain intensity levels were not calibrated in this study.

An estimate of the proportion of FluoroGold-filled vestibular neurons that also contained c-Fos labeling was obtained from images of immunofluorescence-stained sections. All FluoroGold-positive/c-Fos-positive and FluoroGold-positive/c-Fos-negative cells were counted in images from immunofluorescence-stained sections containing at least one double-labeled vestibular neuron. Images from six experiments, utilizing tissue sections from all 10 tracer-injected rats, were examined. Sections from the same animal were separated by at least 250 μm to avoid counting the same neuron twice.

Publication images were prepared using Adobe Photoshop and Illustrator CS6. Adjustments of brightness and contrast were accomplished with the Photoshop Levels and Curves tools applied equally to all parts of each image. For these adjustments, the levels intensity check function was used to optimize the image data range by clipping the background field to zero intensity, with the darkest specimen values just above zero. The curves tool was then used to optimize contrast and tonal mapping. The levels tool was then used again, solely as a

diagnostic, to double check for saturation regions. We did not utilize the Photoshop Autolevels function because this imprecisely uses percentages to judge clipping levels.

Atlas data—The Bregma levels of all stained sections were estimated by comparing the anatomical landmarks with standard rat brain atlas sections (Paxinos and Watson, 2005). Sections stained by immunoperoxidase to identify the FluoroGold injection site were imaged, and the location of the injection site and tracer diffusion penumbra in each animal was plotted manually on brainstem drawings made from these atlas sections. Similarly, all double-labeled (c-Fos and FluoroGold-immunofluorescent) vestibular neurons were imaged and mapped onto standard atlas templates. Data from five rats with injections within RVLM were pooled, as were the data from five rats with injections into CVLM.

RESULTS

Low frequency binaural sGVS was used to stimulate the vestibular nerve and activate the vestibulo-sympathetic pathway. Activated vestibular neurons were observed using immunofluorescence detection of c-Fos in representative Vibratome sections spanning the entire rostro-caudal extent of the VNC. As previously reported, following sGVS, c-Fos-labeled vestibular neurons were observed in SpVN, caudal MVN, throughout the rostrocaudal extent of parvocellular MVN (Fig. 2), and in a small medial wedge of the superior vestibular nucleus (Holstein et al., 2012).

The utility of c-Fos staining for visualizing functionally activated vestibulo-sympathetic pathways was assessed using series' of brainstem sections from sGVS-stimulated and non-stimulated control animals. These tissue sections were processed contemporaneously for immunoperoxidase-DAB immunolabeling, using the same reagents and incubation periods. The glass slide-mounted sections were imaged using the same photomicroscopic conditions, and the subsequent image processing utilized the same decision rules for adjustments of image brightness and contrast. In comparison to the labeling observed in the VNC of sGVS-stimulated rats, brainstem sections from control animals that did not receive sGVS stimulation showed negligible c-Fos immunoreactivity in the vestibular nuclei (Table 2). However, some neurons of the solitary nucleus, gigantocellular reticular nucleus, nucleus ambiguus and the RVLM were immunolabeled in both sGVS-stimulated and non-stimulated control rats (Fig. 3). This labeling presumably reflects ongoing homeostatic neural activity, including the baroreflex, in these cell groups. The few neurons that were immunolabeled in the vestibular nuclei of the non-stimulated rats were scattered throughout the VNC and comprised no more than 4 cells/region/DAB-stained section.

In order to determine whether vestibular neurons directly contribute to pathways controlling blood pressure and heart rate, small iontophoretic injections of the retrograde tracer FluoroGold were placed in the RVLM or CVLM (Fig. 4). FluoroGold was selected as the retrograde tracer based on published reports of its sensitivity, uni-directional transport, and comparatively low probability of uptake by fibers of passage (Raju and Smith, 2006; Schofield, 2008).

Rats were euthanized 10 days after the tracer injection, and a series of Vibratome sections through the caudal medulla, one every 250 μm, was processed for immunoperoxidase labeling of the FluoroGold. The injection site and diffusion penumbra in each rat were then visualized by brightfield microscopy, and mapped onto standard brainstem atlas templates (Paxinos and Watson, 2005). Examples of the tracer injection and diffusion maps in CVLM and RVLM are shown in Figure 5. The full rostro-caudal extent of the injection and penumbra in each of the 10 rats used in this study is presented in Table 3.

Brightfield analysis of these sections confirmed that FluoroGold-filled cell bodies in the VNC are primarily located in the caudal and parvocellular MVN and in SpVN, with a few occasional scattered neurons observed more rostrally in MVN and the superior vestibular nucleus (Fig. 6). Retrogradely filled neurons were not observed in magnocellular MVN. Three cytological types of VNC neurons contained FluoroGold: multipolar (Fig. 6A, B-right, and D), globular (Fig. 6B-left, C and G), and fusiform (Fig. 6E, F and H). These three cell types were not topographically segregated, and were distributed widely through the regions described above. As a group, the multipolar neurons appeared to have the largest cell bodies and largest nuclei, with numerous processes emerging from the somata and multiple secondary and tertiary dendritic branches. The globular neurons were smaller, spheroid, and had fewer primary dendritic processes. The spindle-shaped fusiform neurons had processes emanating from the two tapered ends of the soma, as is seen in cerebral cortex.

The present study tested the hypothesis that sGVS-activated vestibular neurons have direct projections to the RVLM or CVLM. To evaluate this, rats received unilateral iontophoretic FluoroGold tracer injections in one of the two ventral medullary sites, and 10 days later received sGVS stimulation 90 min prior to euthanasia. Tissue sections through the vestibular nuclei were immunostained for c-Fos and FluoroGold and then examined for evidence of co-localization of the two markers. Double-labeled cells were interpreted as neurons that were activated by sGVS *and* sent direct projections to the RVLM or CVLM; such cells were designated “activated projection neurons”.

Activated projection neurons were concentrated in the caudal half of SpVN, caudal MVN, and the caudalmost region of parvocellular MVN. Approximately 78% of the retrogradely filled neurons in this region were also cFos-positive. Activated projection neurons with projections to RVLM (Fig. 7) were found primarily between Bregma −10.80 and −12.84. The highest density of double-labeled neurons was seen at approximately Bregma −11.64, with the majority of activated projection neurons observed at or rostral to this level. While activated projection neurons with terminals in CVLM shared the same overall rostrocaudal distribution (Fig. 8), they were most highly concentrated at Bregma −11.88, and were predominantly located at or caudal to that level. Activated projection neurons with ipsilateral projections were approximately twice as prevalent as those with contralateral terminals in either RVLM or CVLM.

Figures 9–11 illustrate double-labeled cells from each of the two VNC regions projecting to RVLM (Figs. 9 and 10) or CVLM (Fig. 11). All three morphological types of cells observed using retrograde tracing alone were double labeled in SpVN and sent direct projections to

the RVLM (Fig. 9). There were no differences in the cytology of SpVN neurons with ipsilateral (Fig. 9A–D) vs contralateral (Fig. 9E, F) projections. Similarly, there were fusiform (Fig. 10A), multipolar (Fig. 10B, D), and globular (Fig. 10C, D) activated cells in MVN that had direct projections to the ipsilateral (Fig. 11A, B) or contralateral (Fig. 11C, D) RVLM. These three cell types were also identified in SpVN (Fig. 11A–D) and MVN (Fig. 11E–H) projections to ipsilateral (Fig. 11A, B, E and F) and contralateral (Fig. 11C, D, G, and H) CVLM. Together, these findings demonstrate that all vestibular activated projection neurons with ipsilateral and contralateral projections to RVLM or CVLM are small or medium size neurons (10–20 μm diameter) with multipolar, globular or fusiform cytology that are widely distributed throughout the caudal half of SpVN and parvocellular MVN.

DISCUSSION

It is currently understood that arterial baroreceptors participate in a regulatory feedback mechanism that maintains sympathetic tone through the baroreflex while signals from the vestibular end organs drive a more direct feed-forward mechanism that alters blood pressure to counteract the impact of a change in posture on blood flow to the brain (for review, see (Yates and Bronstein, 2005)). By analogy to the better-characterized vestibulo-ocular and -spinal reflexes, this pathway mediating orthotension is often referred to as the vestibulo-sympathetic reflex. The present study provides the first direct visualization of neurons in the MVN and SpVN that are activated by low frequency sGVS and send direct projections to the RVLM or CVLM. We interpret these activated vestibular projection neurons as the central cells of the vestibulo-sympathetic reflex.

Modulations in systemic blood pressure are monitored by baroreceptors in the carotid body and aortic arch. Second order neurons of this baroreflex pathway are located in the solitary nucleus (Spyer, 1981), which sends major projections to the CVLM, and a smaller direct input to the RVLM. The RVLM provides the main excitatory input to preganglionic sympathetic neurons in the intermediolateral cell column of the spinal cord involved in the control of blood pressure (Blessing, 2004; Card et al., 2006; Dampney, 1994; Dampney et al., 1982; Guyenet, 2006; Lipski et al., 1995; Pilowsky and Goodchild, 2002; Reis, 1996; Reis et al., 1988; Ross et al., 1984a; Ross et al., 1984b; Sved et al., 2003; Willette et al., 1983). The CVLM, in contrast, provides both excitatory and inhibitory input to the RVLM (Blessing, 1988; Dampney et al., 2003; Guyenet, 1990; Heesch et al., 2006; Holstege, 1989; Jeske et al., 1995; Natarajan and Morrison, 2000; Pilowsky and Goodchild, 2002; Schreihofer et al., 2005; Stocker et al., 1997), as well as catecholaminergic projections to the hypothalamus and basal forebrain (Chan and Sawchenko, 1998; Cravo et al., 1991; Schreihofer and Guyenet, 2002). Accordingly, cells in the RVLM and CVLM have distinct and diverse roles, extending well beyond the basic circuitry of the baroreflex.

Postural adjustments detected by vestibular receptors, particularly movements involving alterations in head and body position with regard to gravity, evoke sympathetic responses (Carter and Ray, 2008; Tanaka et al., 2009). In humans, caloric vestibular stimulation (Cui et al., 1997), head pitch (Ray and Carter, 2003; Ray et al., 1998) and GVS (Bent et al., 2006; Grewal et al., 2009; James and Macefield, 2010; Voustianiouk et al., 2004; Voustianiouk et

al., 2006) have all been demonstrated to alter sympathetic nerve activity (SNA) (for review, see (Yates and Bronstein, 2005)). Similarly, linear acceleration causes transient changes in blood pressure and blood flow (Cui et al., 1999; Serrador et al., 2009) that are attenuated in patients with bilateral vestibular deficits (Yates et al., 1999). Otolith activation by off-vertical-axis rotation produces an increase in muscle SNA in-phase with the component associated with head-up tilt and a decrease in this activity corresponding to the head-down tilt component (Kaufmann et al., 2002). Together, these studies demonstrate the existence of a functional connection between the vestibular system, particularly the otolith organs, and the sympathetic nervous system.

Among these functional connections, one of the better understood is the vestibular influence on blood pressure (Yates, 1996). The first study in experimental animals demonstrating blood pressure changes in response to postural adjustments was conducted in anesthetized and paralyzed cats, and found orthostatic intolerance during nose-up pitch following bilateral vestibular nerve transection (Doba and Reis, 1974). These findings were subsequently replicated in unanesthetized animals (Abe et al., 2008; Etard et al., 2004; Jian et al., 1999; Nakamura et al., 2009). Moreover, otolith-specific stimulation achieved through linear acceleration (Abe et al., 2009; Yates et al., 1999) or head-up tilt increases SNA (Yates and Miller, 1994) and elevates blood pressure (Woodring et al., 1997), while nose-down stimulation decreases such activity (Nakamura et al., 2009) in experimental animals. Similarly, numerous studies have reported that SNA increases during electrical stimulation of primary vestibular afferents (Cobbold et al., 1968) (for review, see (Yates and Bronstein, 2005)). Thus, data from both humans and experimental animals, including rodents, indicate that vestibular nerve activity contributes to the control of blood pressure (Ray, 2000). However, whereas the effects of bilateral labyrinthectomy on blood pressure control are transient (Yates and Miller, 2009), ablation of the caudal VNC permanently eliminates the decrease in blood pressure that is normally elicited by caloric stimulation (Uchino et al., 1970). This suggests that the caudal VNC is a key site for organizing vestibular (and other sensory) influences on the vestibulo-sympathetic reflex, and is not simply a passive relay.

The present study demonstrates that activated projection neurons of the vestibulo-sympathetic reflex are located in the caudal SpVN, caudal MVN and caudal half of the parvocellular MVN. There is a general topography in the distribution of these activated projection neurons since the cell bodies with terminals in the RVLM are as a group located somewhat more rostrally to those with projections to CVLM. This is noteworthy because the RVLM is the most likely site of convergence of the baroreflex and vestibulo-sympathetic reflex. Although mono- and poly-synaptic pathways from the VNC to CVLM and the solitary nucleus as well as RVLM have been demonstrated (Balaban and Beryozkin, 1994; Holstein et al., 2011; Porter and Balaban, 1997; Ruggiero et al., 1996; Yates et al., 1994), so that convergence of the baroreflex and the vestibulo-sympathetic reflex could happen at any of these sites, functional interactions do not appear to occur in the solitary nucleus or CVLM. Vestibular and baroreceptor terminals fields in the solitary nucleus are largely separate, and lesions there have little effect on sympathetic activity elicited by electrical stimulation of the vestibular nerve (Balaban and Beryozkin, 1994; Steinbacher and Yates, 1996; Yates et al., 1994; Yates and Miller, 1994). In addition, despite the presence of vestibular terminals in both the solitary nucleus and CVLM, neither cell group responds

appreciably to vestibular nerve stimulation. Thus, the solitary nucleus appears to be more functionally specific to the baroreflex (Kerman and Yates, 1998), while CVLM participates in both baroreflex and more complex circuitry in medullary and higher brainstem and forebrain sites. In contrast, RVLM neurons receive significant convergent baroreceptor and vestibular input (Yates and Bronstein, 2005) and inactivation of the RVLM abolishes vestibular nerve stimulation-elicited effects on sympathetic nerve activity (Yates et al., 1995). The present finding that activated projection neurons of the vestibular-sympathetic reflex with projections to RVLM are located more rostrally in the VNC than those to CVLM supports the notion that RVLM and CVLM subserve different functions, and extends this idea to include possible differences in VNC input. One possibility in this regard is that vestibular projections convey a direct, shorter latency input to RVLM to accomplish more rapid changes in blood pressure in response to changes in posture, while the projections to CVLM support a longer latency pathway that distributes vestibular information more widely to the brainstem, hypothalamus and telencephalon. The existence of both short- and long-latency vestibulo-sympathetic reflex pathways has already been suggested on the basis of sympathetic nerve recordings in humans (Voustianiouk et al., 2006).

The present study found that activated projection neurons comprise a large subset of all cells activated by sGVS. GVS has been used for over a century to activate the vestibular system (for review, see (Curthoys, 2010)) without stimulating body tilt receptors or other sensory systems such as proprioception. The cathodal stimulus preferentially activates vestibular afferents with irregular spontaneous firing rates (Goldberg et al., 1984; Minor and Goldberg, 1991), while afferents are inhibited at the anode (for review, see (Fitzpatrick and Day, 2004)). Although the entire labyrinth is activated (Carter and Ray, 2008; Goldberg et al., 1984), the low frequency characteristics of the current steps and the perceptual, ocular, and postural responses that are elicited indicate that the predominant activation is otolithic (Cohen et al., 2011b; 2012; Ray et al., 1998), although semicircular canal-related activity has also been reported (Curthoys and MacDougall, 2012; Shanidze et al., 2012). Macefield and colleagues have clearly demonstrated that sGVS modulates muscle SNA in humans (Bent et al., 2006; Grewal et al., 2012; Grewal et al., 2009; Hammam et al., 2012; Hammam et al., 2011; James and Macefield, 2010; James et al., 2010), further substantiating the utility of this stimulus in activating the VSR.

In the present study, sGVS-activated neurons were visualized using c-Fos immunolabeling. In addition to the activated projection neurons containing labels for both c-Fos and the retrograde tracer, some vestibular neurons in tissue from each animal were c-Fos-positive, but lacked FluoroGold immunofluorescence. Since these data were based on tissue from rats receiving unilateral tracer injections into RVLM or CVLM, many of these single-labeled neurons are likely to be activated projection neurons with ipsilateral projections on the non-injected side of the ventrolateral medulla. However, some c-Fos-positive/FluoroGold negative cells were located more rostrally in parvocellular MVN. These neurons may participate in the projections to the parabrachial nuclei that have been proposed to integrate visceral, emotional and vestibular signals (Balaban, 1996; Kerman et al., 2006).

Our study revealed that activated projection neurons of the vestibulo-sympathetic reflex are scattered throughout the caudal MVN, caudal parvocellular MVN, and caudal SpVN. They

were not preferentially located in the periventricular zone, as has previously been suggested (for review, see (Balaban and Yates, 2004), and were not observed in clusters. As noted above, it is likely that the activated projection neurons receive substantial input from the otolith organs, and probably convergent semicircular canal signals. It has been demonstrated in a number of species that VNC neurons receiving otolith-only or convergent otolith and canal input are widely distributed in the VNC (McArthur et al., 2011) (for review, see (Newlands and Perachio, 2003)). This is in contrast to the horizontal and vertical vestibulo-ocular reflex-related neurons, which are located in discrete, circumscribed clusters (for review, see (Holstein, 2012)). The widespread distribution of activated projection neurons in the caudal VNC appears to reflect the dispersion of otolith-related inputs to this region.

Three very different morphological types of activated projection neurons were observed in this study: multipolar, spherical and fusiform. Based on the success in parsing function by cytology in regions as diverse as the cerebral cortex, neostriatum, thalamus, cerebellum, and spinal cord, we sought to determine whether these three cell types differed in their projections to RVLM vs CVLM, and/or to the ipsilateral vs contralateral medulla. No such differences were observed. One possible explanation for this is that, as in numerous classical neuroanatomical studies of the VNC, cytology alone is not a definitive factor in distinguishing functional pathways in the central vestibular system. However, cytology has been used to some advantage in identifying functional connections in the vestibulo-ocular reflex pathways, as well as in oculomotor-related cell groups (for reviews, see (Büttner-Ennever, 2007; Highstein and Holstein, 2006)). Thus, an alternative and perhaps more likely explanation is that the observed cytological differences correlate with other attributes of the vestibulo-sympathetic reflex-related neurons such as neurotransmitter content, intracellular second messenger systems, and/or neuromodulatory functions.

Methodological considerations

Control experiments for this study included controls for each reagent of the immunolabeling process, and controls for *cfos* activation associated with non-vestibular aspects of the sGVS stimulation paradigm such as stress, handling, electrode placement, and anesthesia. The distribution of c-Fos-labeled cells in this study was qualitatively similar to our previous findings in rats that did not receive FluoroGold injections (Holstein et al., 2012), suggesting that the tracer injection itself did not cause retrograde neuronal degeneration of vestibular neurons, as has been reported in other regions following injections of higher FluoroGold concentrations (Franklin and Druhan, 2000).

The sGVS stimulation was conducted ten days after the FluoroGold tracer injection. Since peak *c-fos* gene activation occurs approximately 30 min after stimulation, and then rapidly declines, it is not likely that the c-Fos protein visualized in this study is attributable to the tracer injection that occurred 10 days earlier. Moreover, the retrograde tracing observed in the present study was comparable to that previously reported (Holstein et al., 2011) so, conversely, the retrograde tracer itself does not appear to be impacted by sGVS stimulation. One conceivable interaction effect, however, is the possibility that the arrival or presence of the FluoroGold tracer in the cell body could itself activate the *cfos* immediate early gene. In our system, however, this is not likely since we observe FluoroGold-positive/c-Fos-negative

neurons in the reticular formation of the same sections that contain double-labeled vestibular neurons.

Approximately 22% of the retrogradely-filled vestibular neurons in double-labeled tissue sections for this study did not show c-Fos labeling. It is possible that there is a parallel pathway from the vestibular nuclei to R/CVLM that does not respond to sGVS, or that some such vestibular cells were not adequately activated by the sGVS stimulus to produce c-Fos protein sufficient for immunofluorescence detection. In addition, it is conceivable that some FluoroGold-only vestibular cells are activated by sGVS, but do not accumulate c-Fos protein because they are rapidly inactivated, most likely by cerebellar Purkinje cell inhibition (Courjon et al., 1987). In fact, it has been reported that neurons receiving substantial tonic inhibitory input do not accumulate c-Fos protein (Chan and Sawchenko, 1994). Nevertheless, the majority (78%) of the FluoroGold-filled somata in the caudal vestibular nuclei were activated by sGVS.

Isoflurane inhalation anesthesia was used for all experiments of the present study. There is some evidence that *c-fos* gene expression is affected by general anesthetics, resulting in increased immediate early gene activity in autonomic nuclei (Hamaya et al., 2000; Roda et al., 2004; Takayama et al., 1994). For example, after 2 hrs exposure to urethane or chloral hydrate anesthesia, both administered i.p., Fos protein expression increased in autonomic brainstem regions associated with blood pressure control in rats (Rocha and Herbert, 1997). However, Fos protein expression remained near baseline after intramuscular ketamine/xylazine administration. When sodium nitroprusside was infused (i.v.) in the ketamine/xylazine anesthetized animals, arterial blood pressure dropped approximately 20 mmHg as expected, and increased numbers of Fos-immunoreactive neurons were subsequently observed in several autonomic nuclei, including the solitary nucleus and ventrolateral medulla. Fos-related immunoreactivity in tissue sections from saline-injected controls was comparable to that of animals receiving ketamine/xylazine injections alone. This study suggests (a) that different anesthetics exert different effects on *c-fos* activation and c-Fos protein expression, and (b) that decreases in blood pressure, as often observed with sGVS, can be accompanied by increased numbers of Fos-immunolabeled neurons in appropriate brainstem regions.

Nevertheless, previous investigators have not found differences between the number of Fos-positive neurons present in limbic areas of brainstem and cerebral cortex of isoflurane anesthetized rats (3% induction, 2% maintenance), compared with unanesthetized subjects (Kufahl et al., 2009). Moreover, while the expression of *c-fos* mRNA in rat brain was significantly higher than baseline after 30 min. exposure to 2% isoflurane, the expression level returned to the control level within 60 min, even though the anesthesia continued for a total of two hours (Hamaya et al., 2000). Thus, isoflurane had no depressant effect on *c-fos* messenger RNA expression in brain, and isoflurane does not appear to alter *c-fos* gene transcription. Based on these reports, and our observation of four or fewer c-Fos positive neurons/region/tissue section in the sGVS control rats, it is not likely that the cFos immunolabeling observed in the sGVS-stimulated vestibular nuclei was due to the isoflurane anesthesia.

Acknowledgments

Grant information: Supported by NIH grant DC008846 from the National Institute on Deafness and Other Communication Disorders.

The authors are grateful to Dr. Ewa Kukielka and Mr. Timothy Mullen for expert technical assistance with this project, and to Dr. Bernard Cohen for valuable discussions about the research and former drafts of this manuscript.

Table of abbreviations used in the figures

12N	hypoglossal nucleus
Cu	cuneate nucleus
CVL(M)	caudal ventrolateral medulla
ECu	external cuneate nucleus
icp	inferior cerebellar peduncle
IML	Intermediolateral cell column
LVe	lateral vestibular nucleus
mlf	medial longitudinal fasciculus
MVe (MVN)	medial vestibular nucleus
MVeMC	medial vestibular nucleus, magnocellular division
MVePC	medial vestibular nucleus, parvocellular division
NTS	Solitary nucleus
Pr; NPH	prepositus nucleus
py	pyramidal tract
RVL(M)	rostral ventrolateral medulla
scp	superior cerebellar peduncle
sol	solitary tract
SolIM	solitary nucleus, intermediate part
sp5	spinal trigeminal tract
Sp5I	spinal trigeminal nucleus, interpolar part
SpVe(N)	spinal vestibular nucleus
SuVe	superior vestibular nucleus
VNC	vestibular nuclear complex
VNCc	Caudal vestibular nuclear complex

Literature Cited

Abe C, Tanaka K, Awazu C, Morita H. Impairment of vestibular-mediated cardiovascular response and motor coordination in rats born and reared under hypergravity. Am J Physiol Regul Integr Comp Physiol. 2008; 295:R173–R180. [PubMed: 18495837]

Abe C, Tanaka K, Awazu C, Morita H. Galvanic vestibular stimulation counteracts hypergravity-induced plastic alteration of vestibulo-cardiovascular reflex in rats. J Appl Physiol. 2009; 107:1089–1094. [PubMed: 19679746]

Angelaki DE, Cullen KE. Vestibular System: The many facets of a multimodal sense. Ann Rev Neurosci. 2008; 31:125–150. [PubMed: 18338968]

Bagnall MW, Stevens RJ, du Lac S. Transgenic mouse lines subdivide medial vestibular nucleus neurons into discrete, neurochemically distinct populations. J Neurosci. 2007; 27(9):2318–2330. [PubMed: 17329429]

Baizer JS, Corwin WL, Baker JF. Otolith stimulation induces c-Fos expression in vestibular and precerebellar nuclei in cats and squirrel monkeys. Brain Research. 2010; 1351:64–73. [PubMed: 20570661]

Balaban CD. Vestibular nucleus projections to the parabrachial nucleus in rabbits: implications for vestibular influences on the autonomic nervous system. Exp Brain Res. 1996; 108:367–381. [PubMed: 8801117]

Balaban CD, Beryozkin G. Vestibular nucleus projections to nucleus tractus solitarius and the dorsal motor nucleus of the vagus nerve: potential substrates for vestibular-autonomic interactions. Exp Brain Res. 1994; 98:200–212. [PubMed: 8050507]

Balaban, CD.; Yates, BJ. Vestibulo-autonomic Interactions: A teleological perspective. In: Highstein, SH.; Fay, RR.; Popper, AN., editors. The Vestibular System. Wein: Springer; 2004. p. 286-342.

Bent LR, Bolton PS, Macefield VG. Modulation of muscle sympathetic bursts by sinusoidal galvanic vestibular stimulation in human subjects. Exp Brain Res. 2006; 174(4):701–711. [PubMed: 16721608]

Blessing WW. Depressor neurons in rabbit caudal medulla act via GABA receptors in rostral medulla. Am J Physiol. 1988; 254:H686–H692. [PubMed: 2833123]

Blessing, WW. Lower brain stem regulation of visceral, cardiovascular, and respiratory function. In: Paxinos, G.; Mai, JK., editors. The Human Nervous System. 2. Amsterdam: Elsevier Academic Press; 2004.

Bourassa EA, Sved AF, Speth RC. Angiotensin modulation of rostral ventrolateral medulla (RVLM) in cardiovascular regulation. Mol Cell Endocrin. 2009; 302:167–175.

Bradbury S, Eggleston C. Postural hypotension. A report of three cases. Am Heart J. 1925; 1:73–86.

Büttner-Ennever, J. Anatomy of the Oculomotor System. In: Straube, A.; Büttner, U., editors. Neuro-Ophthalmology; Neural Control of Eye Movements. Basel: Karger; 2007. p. 1-14.

Cai Y-L, Ma W-L, Li M, Guo J-S, Li Y-Q, Wang L-G, Wang W-Z. Glutamatergic vestibular neurons express Fos after vestibular stimulation and project to the NTS and the PBN in rats. Neurosci Lett. 2007; 417(2):132–137. [PubMed: 17412503]

Cai Y-L, Want J-Q, Chen X-M, Li H-X, Li M, Guo J-S. Decreased Fos protein expression in rat caudal vestibular nucleus is associated with motion sickness habituation. Neurosci Letts. 2010; 480:87–91. [PubMed: 20540989]

Card JP, Sved JC, Craig B, Raizada M, Vazquez J, Sved AF. Efferent projections of rat rostroventrolateral medulla C1 catecholamine neurons: Implications for the central control of cardiovascular regulation. J comp Neurol. 2006; 499:840–859. [PubMed: 17048222]

Carter JR, Ray CA. Sympathetic responses to vestibular activation in humans. Am J Physiol Regul Integr Comp Physiol. 2008; 294(3):R681–688. [PubMed: 18199586]

Chan RK, Sawchenko PE. Spatially and temporally differentiated patterns of c-for expression in brainstem catecholaminergic cell groups induced by cardiovascular challenges in the rat. J comp Neurol. 1994; 348:433–460. [PubMed: 7844257]

Chan RKW, Sawchenko PE. Organization and transmitter specificity of medullary neurons activated by sustained hypertension: implications for understanding baroreceptor reflex circuitry. J Neurosci. 1998; 18(1):371–387. [PubMed: 9412514]

Chen L-W, Lai C-H, Law H-Y, Yung KKL, Chan Y-S. Quantitative study of the coexpression of Fos and N-methyl-D aspartate (NMDA) receptor subunits in otolith-related vestibular nuclear neurons of rats. J comp Neurol. 2003; 460:292–301. [PubMed: 12687692]

Cobbold AF, Megirian D, Sherrey JH. Vestibular evoked activity in autonomic motor outflows. Arch Ital Biol. 1968; 106:113–123. [PubMed: 5681889]

Cohen B, Martinelli GP, Ogorodnikov D, Xiang Y, Raphan T, Holstein GR, Yakushin SB. Sinusoidal galvanic vestibular stimulation (sGVS) induces a vasovagal response in the rat. Exp Brain Res. 2011a; 210(1):45–55. [PubMed: 21374078]

Cohen B, Martinelli GP, Raphan T, Schaffner A, Xiang Y, Holstein GR, Yakushin SB. The vasovagal response of the rat: its relation to the vestibulosympathetic reflex and to Mayer waves. FASEB J. 2013; 27(7):2564–2572. [PubMed: 23504712]

Cohen B, Yakushin SB, Holstein GR. What does galvanic vestibular stimulation actually activate? Front Neurol. 2011b; 2(90):1–2. [PubMed: 21331281]

Cohen B, Yakushin SB, Holstein GR. What does galvanic vestibular stimulation actually activate: response. Front Neurol. 2012; 3:148. [PubMed: 23093948]

Courjon JH, Precht W, Sirkin DW. Vestibular nerve and nuclei unit responses and eye movement responses to repetitive galvanic stimulation of the labyrinth in the rat. Exp Brain Res. 1987; 66(1): 41–48. [PubMed: 3582534]

Cravo SL, Morrison SF, Reis DJ. Differentiation of two cardiovascular regions within caudal ventrolateral medulla. Am J Physiol. 1991; 261(4Pt2):R985–994. [PubMed: 1928446]

Cui J, Iwase S, Mano T, Katayama N, Mori S. Sympathetic response to horizontal linear acceleration in humans. J Gravit Physiol. 1999; 6(1):65–66.

Cui J, Mukai C, Iwase S, Sawasaki N, Kitazawa H, Mano T, Sugiyama Y, Wada Y. Response to vestibular stimulation of sympathetic outflow to muscle in humans. J Auton Nerv Syst. 1997; 66(3):154–162. [PubMed: 9406120]

Curthoys IS. A critical review of the neurophysiological evidence underlying clinical vestibular testing using sound, vibration and galvanic stimuli. Clin Neurophysiol. 2010; 121(2):132–144. [PubMed: 19897412]

Curthoys IS, MacDougall HG. What galvanic vestibular stimulation actually activates. Frontiers in Neurology. 2012; 3:117. [PubMed: 22833733]

Dampney RA. The subretrofacial vasomotor nucleus: Anatomical, chemical and pharmacological properties and role in cardiovascular regulation. Prog Neurobiol. 1994; 42:197–227. [PubMed: 8008825]

Dampney RA, Goodchild AK, Robertson LG, Montgomery W. Role of ventrolateral medulla in vasomotor regulation: a correlative anatomical and physiological study. Brain Res. 1982; 249:223–235. [PubMed: 6128058]

Dampney RA, Horiuchi J, Tagawa T, Fontes MA, Potts PD, Polson JW. Medullary and supramedullary mechanisms regulating sympathetic vasomotor tone. Acta Physiol Scand. 2003; 177(3):209–218. [PubMed: 12608991]

Dieterich, M.; Brandt, T. Functional brain imaging of the vestibular system: fMRI and PET. In: Eggers, SDZ.; Zee, DS., editors. Vertigo and Imbalance: Clinical Neurophysiology of the Vestibular System. Elsevier; 2010.

Doba N, Reis DJ. Role of the cerebellum and vestibular apparatus in regulation of orthostatic reflexes in the cat. Circ Res. 1974; 34:9–18. [PubMed: 4543723]

Durchdewald M, Angel P, Hess J. The transcription factor Fos: a Janus-type regulator in health and disease. Histol Histopathol. 2009; 24:1451–1461. [PubMed: 19760594]

Etard O, Reber A, Quarck G, Normand H, Mulder P, Denise P. Vestibular control of blood pressure during parabolic flights in awake rats. NeuroReport. 2004; 15:2357–2360. [PubMed: 15640755]

Fitzpatrick RC, Day BL. Probing the human vestibular system with galvanic stimulation. J Appl Physiol. 2004; 96:2301–2316. [PubMed: 15133017]

Franklin TR, Druhan JP. The retrograde tracer fluoro-gold interferes with the expression of fos-related antigens. J Neurosci Methods. 2000; 98:1–8. [PubMed: 10837865]

Fuller PM, Jones TA, Jones SM, Fuller CA. Evidence for macular gravity receptor modulation of hypothalamic, limbic and autonomic nuclei. Neurosci. 2004; 129(2):461–471.

Goldberg JM, Smith CE, Fernandez C. Relation between discharge regularity and responses to externally applied galvanic currents in vestibular nerve afferents of the squirrel monkey. J Neurophysiol. 1984; 51(6):1236–1256. [PubMed: 6737029]

Goodchild AK, Moon EA. Maps of cardiovascular and respiratory regions of rat ventral medulla: Focus on the caudal medulla. J Chem Neuroanat. 2009; 38:209–221. [PubMed: 19549567]

Grewal T, Dawood T, Hammam E, Kwok K, Macefield VG. Low-frequency physiological activation of the vestibular utricle causes biphasic modulation of skin sympathetic nerve activity in humans. Exp Brain Res. 2012; 220(2):101–108. [PubMed: 22623094]

Grewal T, James C, Macefield VG. Frequency-dependent modulation of muscle sympathetic nerve activity by sinusoidal galvanic vestibular stimulation in human subjects. Exp Brain Res. 2009; 197:379–386. [PubMed: 19582437]

Gustave Dit Duflo S, Gestreau C, Lacour M. Fos expression in the rat brain after exposure to gravito-inertial force changes. Brain Res. 2000; 861:333–344. [PubMed: 10760495]

Guyenet, PG. Role of ventral medulla oblongata in blood pressure regulation. In: Loewy, AD., editor. Central Regulation of Autonomic Function. New York: Oxford University Press; 1990. p. 145-167.

Guyenet PG. The sympathetic control of blood pressure. Nat Rev Neurosci. 2006; 7:335–346. [PubMed: 16760914]

Hamaya Y, Takeda T, Dohl S, Nakashima S, Nozawa Y. The effects of pentobarbital, isoflurane, and propofol on immediate early gene expression in the vital organs of the rat. Anesthesia and Analgesia. 2000; 90:1177–1183. [PubMed: 10781476]

Hammam E, Dawood T, Macefield VG. Low-frequency galvanic vestibular stimulation evokes two peaks of medulation in skin sympathetic nerve activity. Exp Brain Res. 2012; 219:441–446. [PubMed: 22526950]

Hammam E, James C, Dawood T, Macefield VG. Low-frequency sinusoidal galvanic stimulation of the left and right vestibular nerves reveals two peaks of modulation in muscle sympathetic nerve activity. Exp Brain Res. 2011; 213(4):507–514. [PubMed: 21800255]

Heesch CM, Laiprasert JD, Kvochina L. RVLM glycine receptors mediate GABAa and GABAb independent sympathoinhibition from CVLM in rats. Brain Res. 2006; 1125:46–59. [PubMed: 17112484]

Highstein, SM.; Holstein, GR. The anatomy of the vestibular nuclei. In: Büttner-Ennever, JA., editor. Neuroanatomy of the Oculomotor System. Amsterdam: Elsevier; 2006. p. 157-203.

Holstege G. Anatomical study of the final common pathway for vocalization in the cat. J Comp Neurol. 1989; 284:242–252. [PubMed: 2754035]

Holstein, GR. The Vestibular System. In: Mai, J.; Paxinos, G., editors. The Human Nervous System. 3. London: Elsevier; 2012. p. 1239-1269.

Holstein GR, Friedrich VLJ, Kang T, Kukielka E, Martinelli GP. Direct projections from the caudal vestibular nuclei to the ventrolateral medulla in the rat. Neurosci. 2011; 175:104–117.

Holstein GR, Friedrich VLJ, Martinelli GP, Ogorodnikov D, Yakushin SB, Cohen B. Fos expression in neurons of the rat vestibulo-autonomic pathway activated by sinusoidal galvanic vestibular stimulation. Frontiers in Neurology. 2012; 3(4):1–12. [PubMed: 22279441]

Imholtz BP, Wieling W, Langewouters GJ, van Montfrans GA. Continuous finger arterial pressure: utility in the cardiovascular laboratory. Clin Auton Res. 1991; 1(1):43–53. [PubMed: 1821665]

James C, Macefield VG. Competitive interactions between vestibular and cardiac rhythms in the modulation of muscle sympathetic nerve activity. Autonom Neurosci. 2010; 158(1–2):127–131.

James C, Statis A, Macefield VG. Vestibular and pulse-related modulation of skin sympathetic nerve activity during sinusoidal galvanic vestibular stimulation in human subjects. Exp Brain Res. 2010; 202(2):291–298. [PubMed: 20041236]

Jeske I, Reis DJ, Milner TA. Neurons in the barosensory area of the caudal ventrolateral medulla project monosynaptically on to sympathoexcitatory bulbospinal neurons in the rostral ventrolateral medulla. Neurosci. 1995; 65(2):343–353.

Jian BJ, Cotter LA, Emanuel BA, Cass SP, Yates BJ. Effects of bilateral vestibular lesions on orthostatic tolerance in awake cats. J Appl Physiol. 1999; 86:1552–1560. [PubMed: 10233117]

Kaufman GD. Fos expression in the vestibular brainstem: What one marker can tell us about the network. Brain Res Rev. 2005; 50:200–211. [PubMed: 16039721]

Kaufman GD, Anderson JH, Beitz AJ. Fos-defined activity in rat brainstem following centripetal acceleration. J Neurosci. 1992; 12(11):4489–4500. [PubMed: 1432106]

Kaufman GD, Anderson JH, Beitz AJ. Otolith-brainstem connectivity - evidence for differential neural activation by vestibular hair cells based on quantification of FOS expression in unilateral labyrinthectomized rats. J Neurophysiol. 1993; 70:117–127. [PubMed: 8395570]

Kaufman GD, Perachio AA. Translabyrinthine electrical stimulation for the induction of immediate-early genes in the gerbil brainstem. Brain Res. 1994; 646:345–350. [PubMed: 8069688]

Kaufmann H, Biaggioni I, Voustianiouk A, Diedrich A, Costa F, Clarke R, Gizzi M, Raphan T, Cohen B. Vestibular control of sympathetic activity. An otolith-sympathetic reflex in humans. Exp Brain Res. 2002; 143:463–469. [PubMed: 11914792]

Kerman IA, Akil H, Watson SJ. Rostral elements of sympatho-motor circuitry: A virally mediated transsynaptic tracing study. J Neurosci. 2006; 26(13):3423–3433. [PubMed: 16571749]

Kerman IA, Yates BJ. Regional and functional differences in the distribution of vestibulosympathetic reflexes. Am J Physiol. 1998; 275:R824–R835. [PubMed: 9728081]

Kodama T, Guerrero S, Shin M, Moghadam SH, Faulstich M, Du Lac S. Neuronal classification and marker gene identification via single-cell expression profiling of brainstem vestibular neurons subserving cerebellar learning. J Neurosci. 2012; 32(23):7819–7831. [PubMed: 22674258]

Kovács KJ. Measurement of immediate-early gene activation- c-fos and beyond. J Neuroendocrinol. 2008; 20:665–672. [PubMed: 18601687]

Kufahl PR, Pentkowski NS, Heintzelman K, Neisewander JL. Cocaine-induced Fos expression is detectable in the frontal cortex and striatum of rats under isoflurance but not a-chloralose anesthesia: Implications for FMRI. J Neurosci Methods. 2009; 181:241–248. [PubMed: 19467261]

Lai C-H, Tse Y-C, Shum DKY, Yung KKL, Chan Y-S. Fos expression in otolith-related brainstem neurons of postnatal rats following off-vertical axis rotation. J comp Neurol. 2004; 470:282–296. [PubMed: 14755517]

Lai S-K, Lai C-H, Tse Y-C, Yung KKL, Shum DKY, Chan Y-S. Developmental maturation of ionotropic glutamate receptor subunits in rat vestibular nuclear neurons responsive to vertical linear acceleration. Eur J Neurosci. 2008; 28:2157–2172. [PubMed: 19046363]

Lai S-K, Lai C-H, Yung KKL, Shum DKY, Chan Y-S. Maturation of otolith-related brainstem neurons in the detection of vertical linear acceleration in rats. Eur J Neurosci. 2006; 23:2431–2446. [PubMed: 16706850]

Lipski J, Kanjhan R, Kruszewska B, Smith M. Barosensitive neurons in the rostral ventrolateral medulla of the rat in vivo: morphological properties and relationship to C1 adrenergic neurons. Neurosci. 1995; 69:601–618.

Marshburn TH, Kaufman GD, Purcell IM, Perachio AA. Saccule contribution to immediate early gene induction in the gerbil brainstem with posterior canal galvanic or hypergravity stimulation. Brain Res. 1997; 761:51–58. [PubMed: 9247065]

McArthur KL, Zakir M, Haque A, Dickman JD. Spatial and temporal characteristics of vestibular convergence. Neurosci. 2011; 192:361–371.

Minor LB, Goldberg JM. Vestibular-nerve inputs to the vestibulo-ocular reflex: a functional-ablation study in the squirrel monkey. J Neurosci. 1991; 11(6):1636–1648. [PubMed: 2045879]

Nakamura Y, Matsuo S, Hosogai M, Kawai Y. Vestibular control of arterial blood pressure during head-down postural change in anesthetized rabbits. Exp Brain Res. 2009; 194:563–570. [PubMed: 19225770]

Natarajan M, Morrison SF. Sympathoexcitatory CVLM neurons mediate responses to caudal pressor area stimulation. Am J Physiol Regulatory Integ Comp Physiol. 2000; 279:R364–R374.

Newlands SD, Perachio AA. Central projections of the vestibular nerve: a review and single fiber study in the Mongolian gerbil. Brain Res Bull. 2003; 60:475–495. [PubMed: 12787868]

Paxinos, G.; Watson, C. The Rat Brain in Stereotaxic Coordinates. London: Academic Press; 2005.

Paxinos, G.; Watson, C. The Rat Brain in Stereotaxic Coordinates. London: Academic Press; 2009.

Pilowsky PM, Goodchild AK. Baroreceptor reflex pathways and neurotransmitters: 10 years on. J Hypertens. 2002; 20:1675–1688. [PubMed: 12195099]

Pompeiano O, d'Ascanio P, Centini C, Pompeiano M, Balaban E. Gene expression in rat vestibular and reticular structures during and after space flight. Neurosci. 2002; 114:135–155.

Porter JD, Balaban CD. Connections between the vestibular nuclei and regions that mediate autonomic function in the rat. J Vest Res. 1997; 7:63–76.

Raju DV, Smith Y. Anterograde axonal tract tracing. Curr Protoc Neurosci. 2006; Chapter 1(Unit 1.14)

Ray CA. Interaction of the vestibular system and baroreflexes on sympathetic nerve activity in humans. Am J Physiol Heart Circ Physiol. 2000; 279:H2399–H2404. [PubMed: 11045977]

Ray CA, Carter JR. Review: Vestibular activation of sympathetic nerve activity. Acta Physiol Scand. 2003; 177:313–319. [PubMed: 12609001]

Ray CA, Hume KM, Steele SL. Sympathetic nerve activity during natural stimulation of horizontal semicircular canals in humans. Am J Physio. 1998; 275:R1274–R1278.

Reis DJ. Neurons and receptors in the rostroventrolateral medulla mediating the antihypertensive actions of drugs acting at imidazoline receptors. J Cardiovasc Pharmacol. 1996; 27 (Suppl 3):S11–S18. [PubMed: 8872295]

Reis DJ, Morrison SF, Ruggiero D. The C1 area of the brainstem in tonic and reflex control of blood pressure. Hypertens. 1988; 11(Suppl 1):I8–I13.

Rocha MJA, Herbert H. Effects of anesthetics on Fos protein expression in autonomic brain nuclei related to cardiovascular regulation. Neuropharmacol. 1997; 36(11/12):1779–1781.

Roda F, Pio J, Bianchi A-L, Gestreau C. Effects of anesthetics on hypoglossal nerve discharge and c-Fos expression in brainstem hypoglossal premotor neurons. J comp Neurol. 2004; 468:571–586. [PubMed: 14689487]

Ross CA, Ruggiero DA, Joh TH, Park DH, Reis DJ. Rostral ventrolateral medulla: selective projections to the thoracic autonomic cell column from the region containing C1 adrenaline neurons. J Comp Neurol. 1984a; 228(2):168–185. [PubMed: 6480910]

Ross CA, Ruggiero DA, Park DH, Joh TH, Sved AF, Fernandez-Pardal J, Saavedra JM, Reis DJ. Tonic vasomotor control by the rostral ventrolateral medulla: Effect of electrical or chemical stimulation of the area containing C1 adrenaline neurons on arterial pressure, heart rate, and plasma catecholamines and vasopressin. J Neurosci. 1984b; 4(2):474–494. [PubMed: 6699683]

Ruggiero DA, Mtui EP, Otake K, Anwar M. Vestibular afferents to the dorsal vagal complex: substrate for vestibulo-autonomic interactions in the rat. Brain Res. 1996; 743:294–302. [PubMed: 9017258]

Saxon DW, Anderson JH, Beitz AJ. Transtympanic tetrodotoxin alters the VOR and Fos labeling in the vestibular complex. NeuroReport. 2001; 12:3051–3055. [PubMed: 11568635]

Schofield BR. Retrograde axonal tracing with fluorescent markers. Curr Protoc Neurosci. 2008; 43(Apr) Chapter 1: Unit 1.17.

Schreihofer AM, Guyenet PG. The baroreflex and beyond: control of sympathetic vasomotor tone by GABAergic neurons in the ventrolateral medulla. Clin Exp Pharmacol Physiol. 2002; 29:514–521. [PubMed: 12010201]

Schreihofer AM, Ito S, Sved AF. Brain stem control of arterial pressure in chronic arterial baroreceptor-denervated rats. Am J Physio. 2005; 289:R1746–1755.

Serrador JM, Schlegel TT, Black FO, Wood SJ. Vestibular effects on cerebral blood flow. BMC Neurosci. 2009; 10:119–127. [PubMed: 19775430]

Shanidze N, Lim K, Dye J, King WM. Galvanic stimulation of the vestibular periphery in guinea pigs during passive whole body rotation and self-generated head movement. J Neurophys. 2012; 107:2260–2270.

Spyer KM. Neural organisation and control of the baroreceptor reflex. Rev Physiol Biochem Pharmacol. 1981; 88:24–124. [PubMed: 7010509]

Steinbacher BC, Yates BJ. Processing of vestibular and other inputs by the caudal ventrolateral medullary reticular formation. Am J Physiol. 1996; 271:R1070–R1077. [PubMed: 8898002]

Stocker SD, Steinbacher BC, Balaban CD, Yates BJ. Connections of the caudal ventrolateral medullary reticular formation in the cat brainstem. Exp Brain Res. 1997; 116:270–282. [PubMed: 9348126]

Sved AF, Ito S, Sved JC. Brainstem mechanisms of hypertension: Role of the rostral ventrolateral medulla. Curr Hypertens Rep. 2003; 5:262–268. [PubMed: 12724060]

Takayama K, Suzuki T, Miura M. The comparison of effects of various anesthetics on expression of Fos protein in the rat brain. Neurosci Letts. 1994; 176:59–62. [PubMed: 7970238]

Tanaka K, Abe C, Awazu C, Morita H. Vestibular system plays a significant role in arterial pressure control during head-up tilt in young subjects. Autonom Neurosci. 2009; 148:90–96.

Tse Y-C, Lai C-H, Lai S-K, J-ZL, Yung KKL, DKYS, Chan Y-S. Developmental expression of NMDA and AMPA receptor subunits in vestibular nuclear neurons that encode gravity-related horizontal orientations. J comp Neurol. 2008; 508:343–364. [PubMed: 18335497]

Uchino Y, Kudo N, Tsuda K, Iwamura Y. Vestibular inhibition of sympathetic nerve activities. Brain Res. 1970; 22:195–206. [PubMed: 5458666]

Voustianiouk A, Diedrich A, Ogorodnikov D, MacDougall HG, Raphan T, Biaggioni I, Cohen B, Kaufmann H. Vestibular nerve stimulation modulates muscle sympathetic nerve activity in humans. Clin Auton Res. 2004; 14:335.

Voustianiouk A, Kaufmann H, Diedrich A, Raphan T, Biaggioni I, MacDougall H, Ogorodnikov D, Cohen B. Electrical activtion of the human vestibulo-sympathetic reflex. Exp Brain Res. 2006; 171(2):251–261. [PubMed: 16308690]

Willette RN, Barcas PP, Krieger AJ, Sapru HN. Vasopressor and depressor areas in the rat medulla. Identification by microinjection of L-glutamate. Neuropharm. 1983; 22:1071–1079.

Woodring SF, Rossiter CD, Yates BJ. Pressor response elicited by nose-up vestibular stimulation in cats. Exp Brain Res. 1997; 113:165–168. [PubMed: 9028786]

Yates BJ. Vestibular influences on the autonomic nervous system. Ann NY Acad Sci. 1996; 781:458–473. [PubMed: 8694435]

Yates BJ, Aoki M, Burchill P, Bronstein AM, Gresty MA. Cardiovascular responses elicited by linear acceleration in humans. Exp Brain Res. 1999; 125:476–484. [PubMed: 10323294]

Yates BJ, Bronstein AM. The effects of vestibular system lesions on autonomic regulation: Observations, mechanisms, and clinical implications. J Vest Res. 2005; 15:119–129.

Yates BJ, Grélot L, Kerman IA, Balaban CD, Jakus J, Miller AD. Organization of vestibular inputs to nucleus tractus solitarius and adjacent structures in cat brain stem. Am J Physiol. 1994; 267:R974–R983. [PubMed: 7524372]

Yates BJ, Miller AD. Properties of sympathetic reflexes elicited by natural vestibular stimulation: implications for cardiovascular control. J Neurophysiol. 1994; 71:2087–2092. [PubMed: 7931504]

Yates BJ, Miller DM. Integration of nonlabyrinthine inputs by the vestibular system: role in compensation following bilateral damage to the inner ear. J Vestib Res. 2009; 19(5–6):183–189. [PubMed: 20495235]

Yates BJ, Siniaia MS, Miller AD. Descending pathways necessary for vestibular influences on sympathetic and inspiratory outflow. Am J Physiol. 1995; 268:R1381–R1385. [PubMed: 7611512]

Zhang FX, Lai CH, Tse YC, Shum DKY, Chan YS. Expression of Trk receptors in otolith-related neurons in the vestibular nucleus of rats. Brain Res. 2005; 1062(1–2):92–100. [PubMed: 16256078]

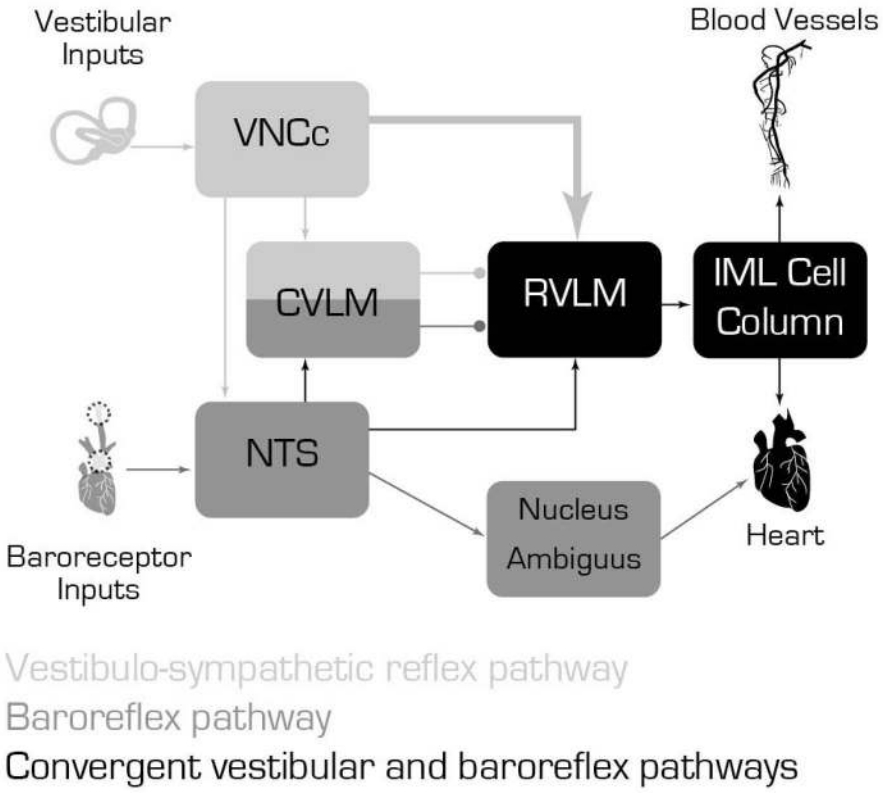

Figure 1.

Schematic diagram illustrating the main cell groups and pathways mediating the interaction between the vestibulo-sympathetic reflex (light gray) and the baroreflex pathway (dark gray). Convergence of these two pathways (black) appears to occur in the RVLM. The large arrow from the VNCc to the RVLM illustrates the activated vestibular projection neurons.

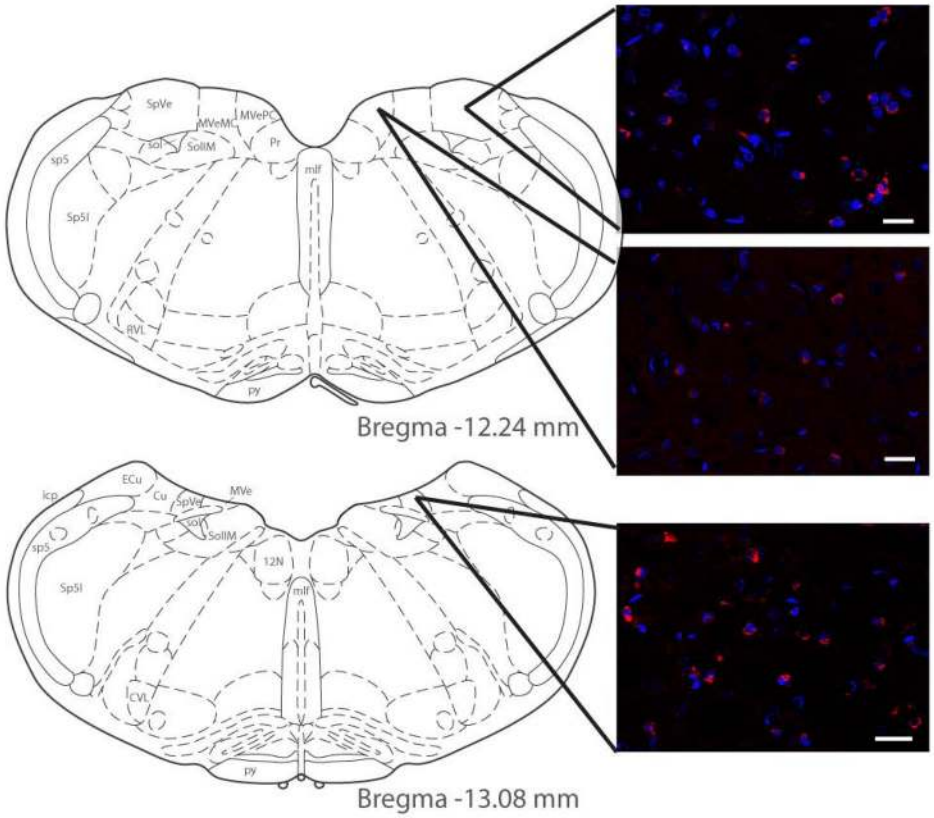

Figure 2.

C-Fos protein (red) visualized by immunofluorescence staining of vestibular neurons activated using low frequency sinusoidal galvanic vestibular stimulation (sGVS). Activated vestibular neurons are illustrated at two levels of the vestibular nuclear complex (VNC), and in both the spinal and medial vestibular nuclei (SpVN and MVN, respectively). DAPI (blue) was used as a marker for neuronal nuclei. As previously reported (Holstein et al., 2012), c-Fos-positive vestibular neurons were observed in the caudal half of SpVN and throughout the non-magnocellular MVN after sGVS stimulation. Atlas templates were obtained from (Paxinos and Watson, 2005). Scale bars: 20 μm.

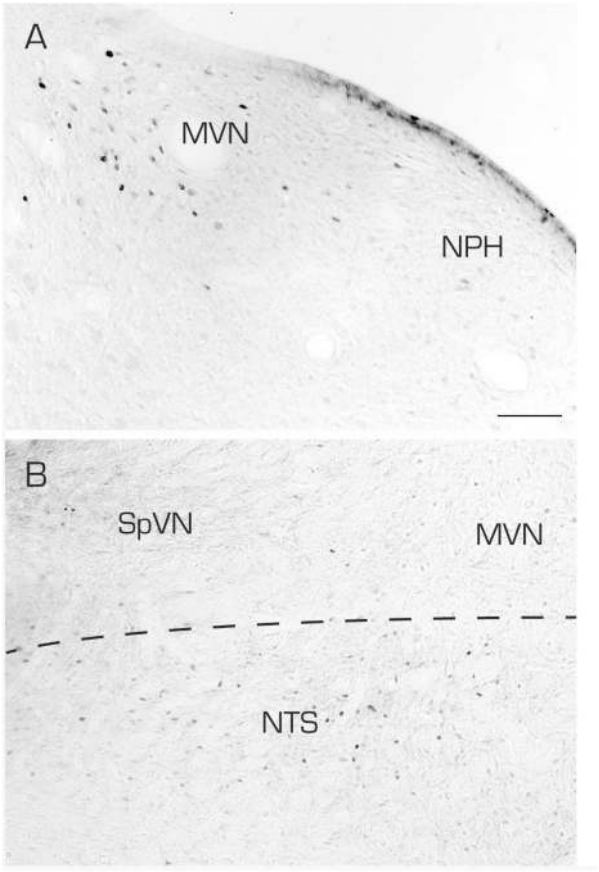

Figure 3.

Vibratome sections from an sGVS-stimulated (A) and a non-stimulated (B) rat, processed identically and contemporaneously for immunoperoxidase/diaminobenzidine staining of c-Fos protein. A: The sGVS stimulation resulted in substantial accumulation of c-Fos protein in neurons in MVN but not the prepositus nucleus (NPH). B. In the non-stimulated rat, c-Fos-immunoreactive neuronal nuclei were apparent in the solitary nucleus (NTS), but rarely in SpVN or MVN. In both panels, the midline is to the right. Scale bar in A is for both panels: 100 μm.

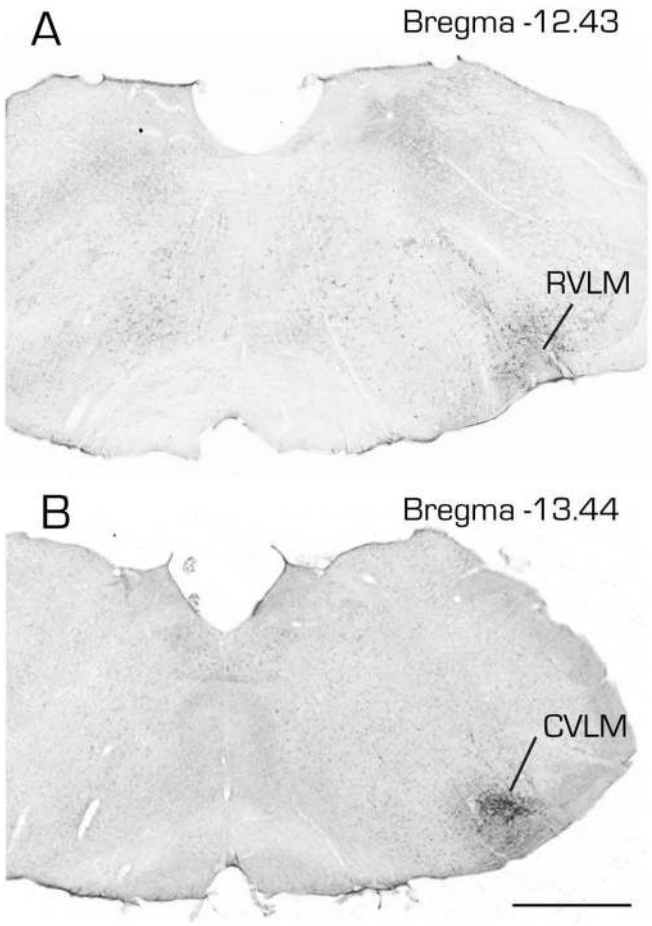

Figure 4.

Photomicrographs of immunoperoxidase/diaminobenzidine-stained Vibratome sections from two rats, one with a FluoroGold tracer injection into RVLM (A) and the other with a similar tracer injection into CVLM (B). Estimated Bregma levels are based on matching anatomical boundaries with atlas drawing from (Paxinos and Watson, 2005). Scale bar in B: 1 mm for both panels.

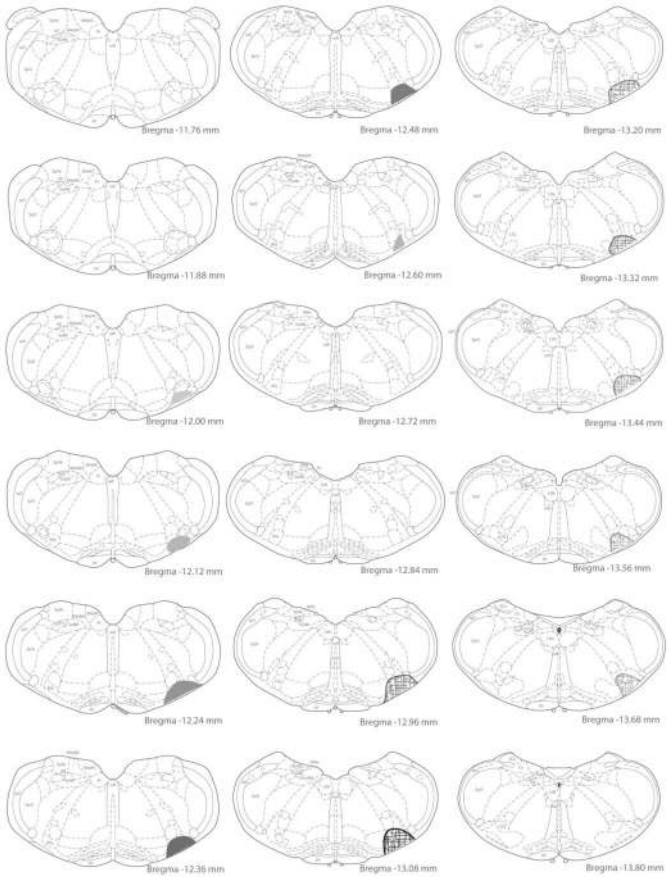

Figure 5.

Examples of injection site maps. The location of the injection site and extent of the local diffusion of tracer was identified in each animal using immunoperoxidase/diaminobenzidine-stained sections through the medulla. This site was then plotted on drawings of rat brain stereotaxic atlas sections (Paxinos and Watson, 2005) by matching the anatomical structures present on the ventral aspect of stained sections to the atlas images. In the two rats depicted in the figure, the injection site in the rostral ventrolateral medullary region (RVLM) extended from Bregma −12.00 to −12.66 and is illustrated by filled shapes; the injection site in the caudal ventrolateral medulla (CVLM) extended from Bregma −12.9 to −13.68 and is illustrated with hatchmark-filled shapes. For both injection sites, the shading opacity reflects the density of the labeling observed in the tissue sections.

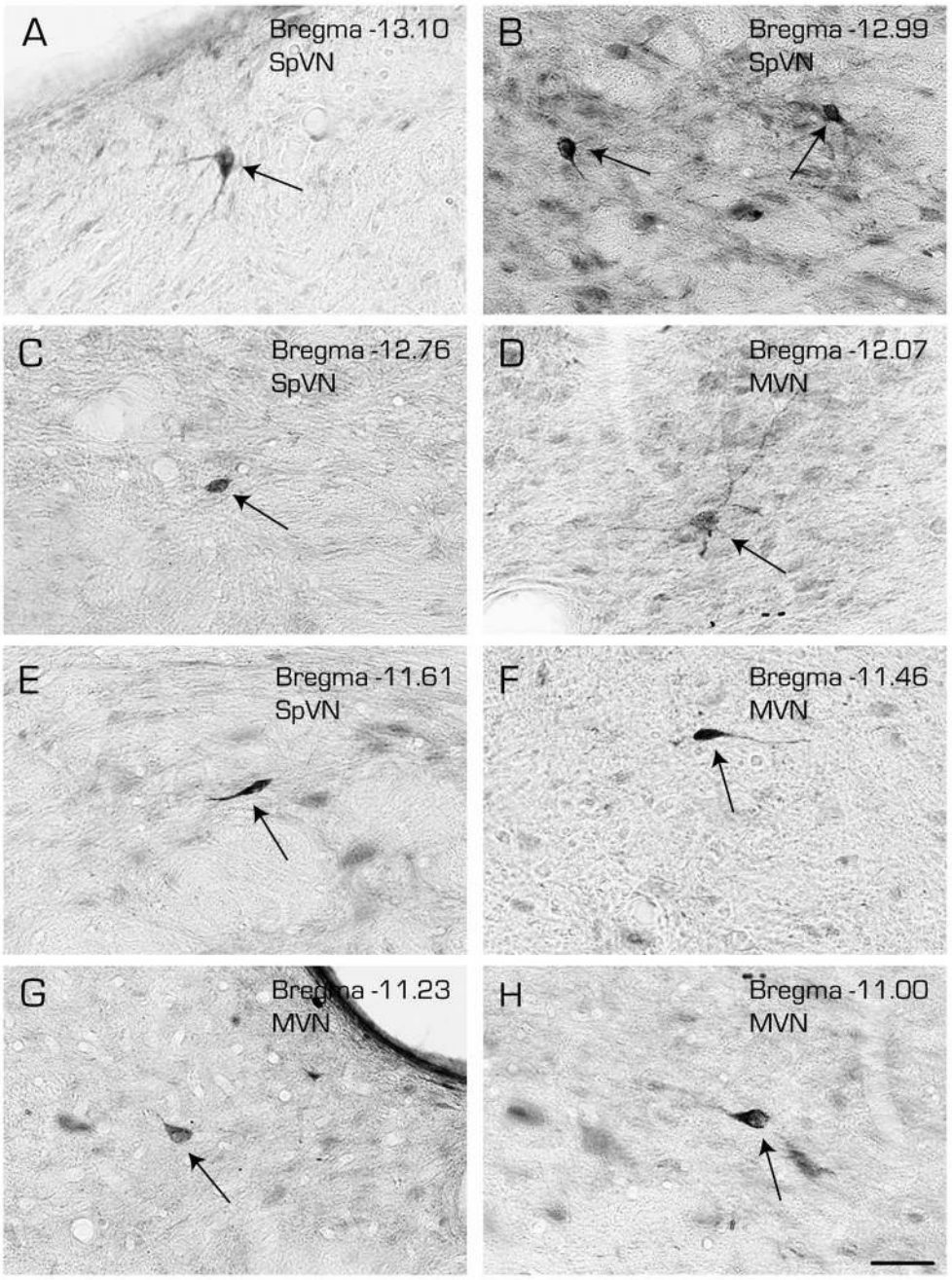

Figure 6.

Immunoperoxidase/diaminobenzidine-stained Vibratome sections through the caudal vestibular nuclei illustrating the three morphological types of vestibular neurons that were retrogradely-filled following a FluoroGold tracer injection into CVLM. Multipolar (A, B-right, D), globular (B-left, C and G) and fusiform (E, F and H) cells (arrows) were observed throughout the caudal half of SpVN and through the caudal and parvocellular MVN. Estimated Bregma levels are based on matching anatomical boundaries with atlas drawing from (Paxinos and Watson, 2005). Scale bar in H: 50 μm for all panels.

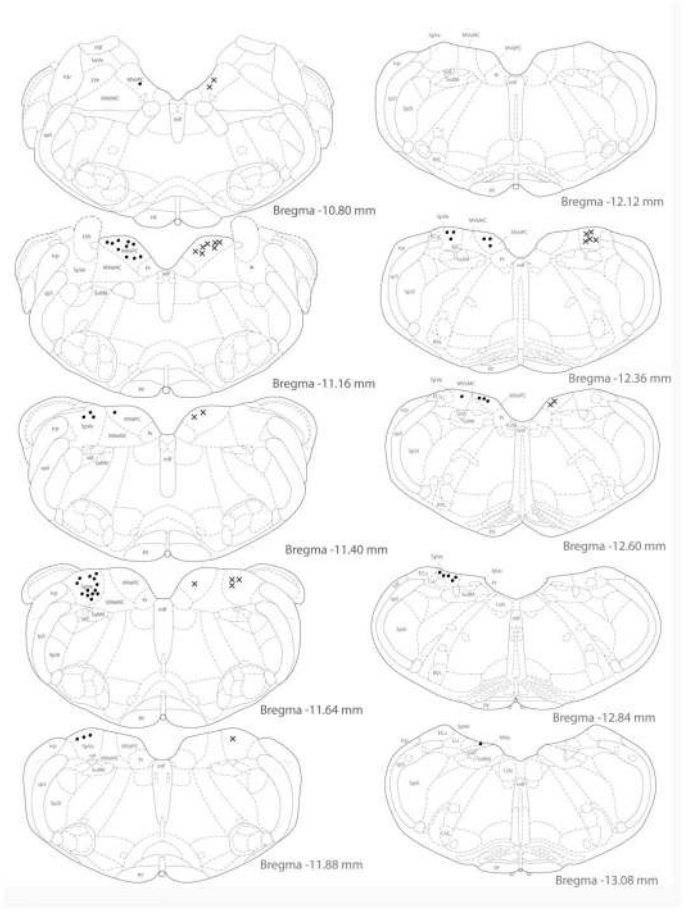

Figure 7.

Location of vestibular neurons that were activated by sGVS and had direct projections to the ipsilateral (filled circles on left side of each drawing) or contralateral (Xs on right side of each drawing) RVLM. The highest density of activated vestibular neurons with direct projections to RVLM was observed at Bregma −11.64, and the majority of these activated projection neurons were observed at or rostral to this level.

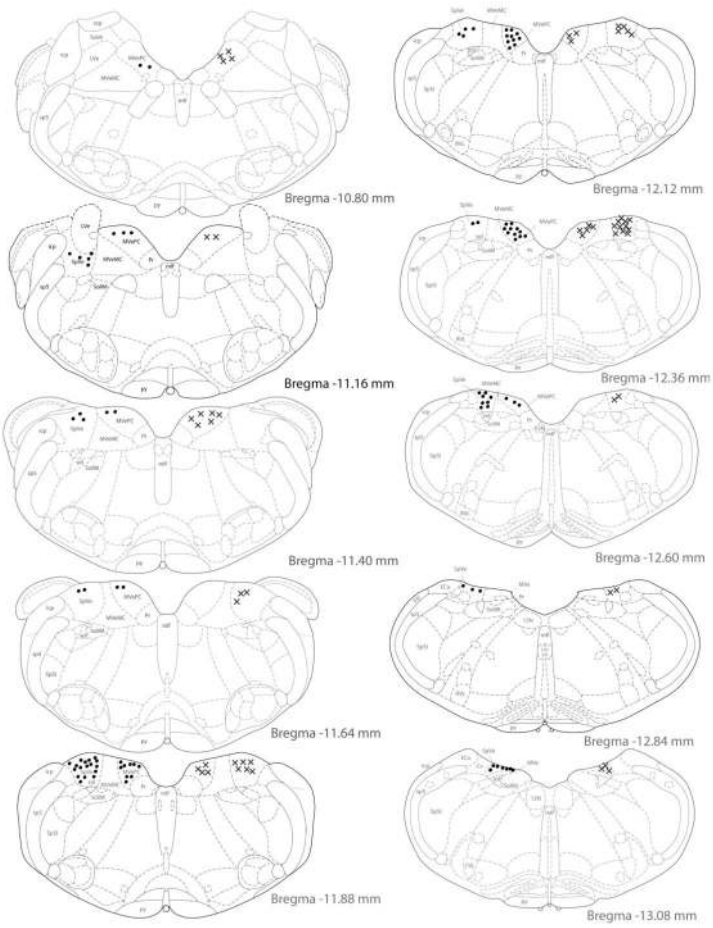

Figure 8.

Location of vestibular neurons that were activated by sGVS and had direct projections to the ipsilateral (filled circles on left side of each drawing) or contralateral (Xs on right side of each drawing) CVLM. The highest density of cells was observed at Bregma −11.88, with most of these activated projection neurons observed at or caudal to this level.

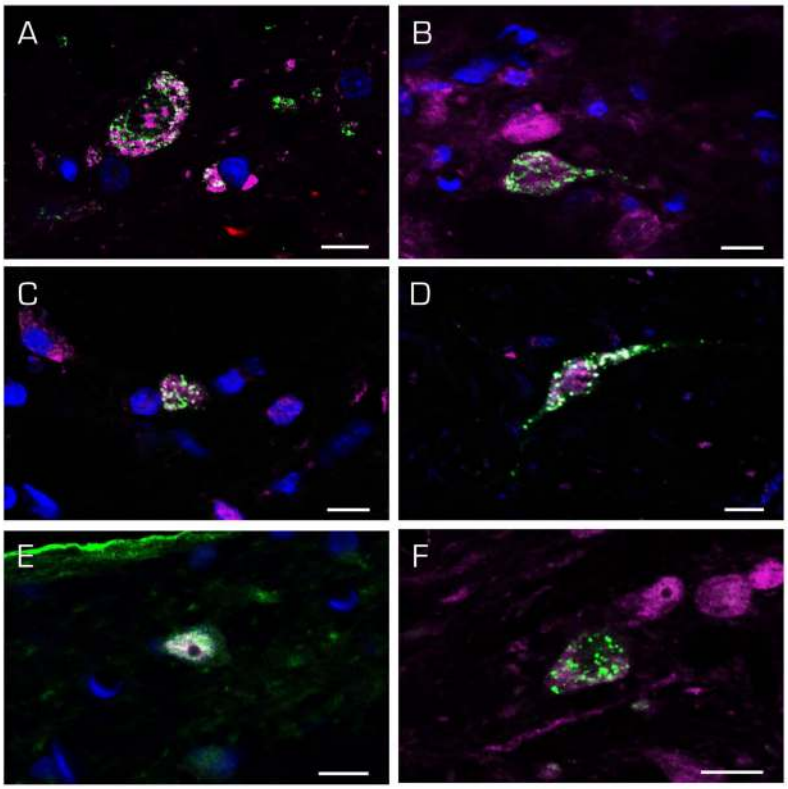

Figure 9.

Immunofluorescence images of c-Fos-positive (magenta) SpVN neurons with direct projections to RVLM. The FluoroGold tracer (green) has a punctate appearance in the somata and dendrites of retrogradely-filled neurons. Multipolar (A, B, F), globular (C, E) and fusiform (D) neurons were observed, and there were no differences in the cytology of neurons projecting ipsilaterally (A–D) vs contralaterally (E–F). Scale bar in each panel: 10 μm.

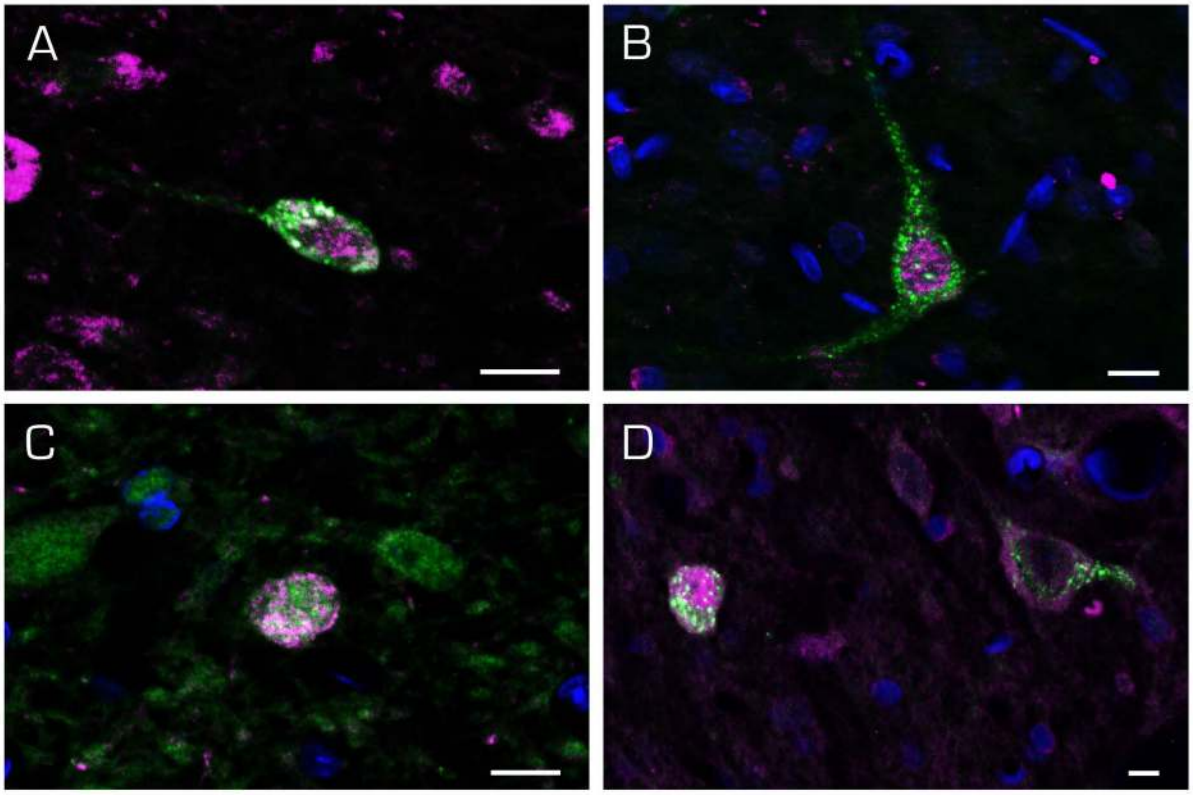

Figure 10.

Examples of c-Fos (magenta) and FluoroGold (green) labeled vestibular neurons in MVN neurons with direct projections to RVLM. Fusiform (A), multipolar (B, D, right), and globular (C, D left) neurons were observed, as were activated projection neurons with ipsilateral (A, B) and contralateral (C, D) projections. Scale bar in each panel: 10 μm

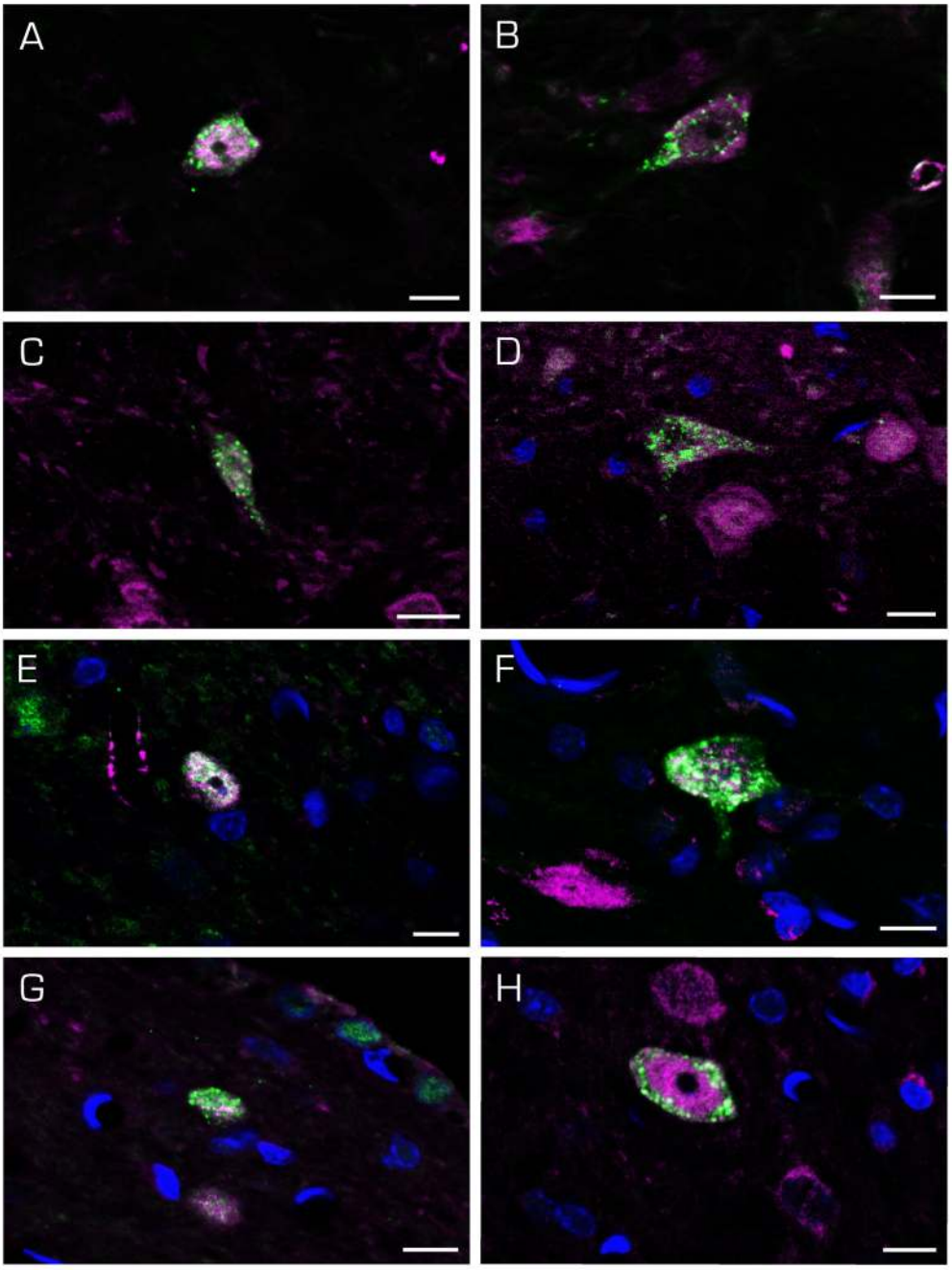

Figure 11.

Immunofluorescence images of c-Fos-positive (magenta) SpVN neurons (A–D) and MVN neurons (E–H) with direct projections to the CVLM (FluoroGold; green). Cells with ipsilateral (A, B, E, F) and contralateral (C, D, G, H) terminal fields were observed. Scale bar in each panel: 10 μm.

Table 1

Primary antibodies used in this study

Antigen	Host and Type	Immunogen	Source	Working dilutions
c-Fos	Rabbit polyclonal	A peptide mapping within an internal region of human c-Fos	Santa Cruz Biotech; Cat. # Sc-253	1:500
c-Fos-488	Rabbit polyclonal	A peptide mapping within an internal region of human c-Fos	Santa Cruz Biotech; Cat. # Sc-253AF488	1:10, 1:50, 1:100, 1:200, 1:500, 1:1000
c-Fos	Rabbit polyclonal	A synthetic peptide (SGFNADYEASSSRC) corresponding to amino acids 4–17 of human c-Fos	Calbiochem; Cat. # PC38	1:500, 1:1000, 1:10,000, 1:50,000
FluoroGold	Rabbit polyclonal	Fluorogold	Millipore; Cat. # AB153	1:400 (IMF); 1:5000 (DAB)

Table 2

Number of c-Fos-positive cells in the vestibular nuclei with and without sGVS

	MVN	SpVN
sGVS	41 ± 15 *	33 ± 13 *
Unstimulated control	1.5 ± 0.7	1.7 ± 0.7

Number of c-Fos-positive neurons per 50 μm Vibratome section in MVN and SpVN (mean ± SEM).

* Significantly different from unstimulated control ($p<0.004$, t-test).

Table 3

FluoroGold injection sites

	Caudal	Center	Rostral
RVLM			
R687	−12.28	−11.90	−11.78
R696	−12.57	−12.11	−11.88
R698	−12.66	−12.43	−12.12
R700	−12.84	−12.66	−12.36
R701A	−12.84	−12.36	−12.12
CVLM			
R688	−13.66	−13.41	−13.16
R690	−13.68	−13.43	−12.93
R695	−13.56	−13.22	−12.30
R697	−13.44	−13.20	−12.96
R702	−13.68	−12.96	−12.80

Bregma levels of the tracer injection site (Center) and the rostral and caudal extent of the tracer diffusion in RVLM or CVLM of all rats used for the double label immunofluorescence studies. Based on the most conservative estimates, RVLM extends from Bregma −11.8 to −12.8 and CVLM extends from Bregma −12.8 to −13.6.